PSS performance monitoring and PSS redesign based on system identification techniques

Xavier Bombois, Luigi Vanfretti

PSS performance monitoring and PSS redesign based on system identification techniques

Xavier Bombois[a,b], Luigi Vanfretti[c]

[a]*Laboratoire Ampere, Ecole Centrale de Lyon, Universite de Lyon, Ecully, France*
[b]*Centre National de la Recherche Scientifique (CNRS), France*
[c]*Department of Electrical, Computer, and Systems Engineering, Rensselaer Polytechnic Institute, Troy, NY, USA*

Abstract

To maintain stable power system operation, damping control systems are used in conventional power plants, known as Power System Stabilizers (PSS). However, to derive suitable controller parameters, the current methods require dynamic models that are difficult to maintain and update, and in some cases, might not be available. This makes it challenging for grid operators to maintain system stability when the system is under stringent operating conditions or undergoes the loss of major transmission corridors, which would require a new stabilizer design to provide adequate damping.

Leveraging the availability of real-time measurements and "probing" technologies, this paper provides a complementary approach that does not require power system simulation models, but is based on system identification techniques that allow to derive simple and accurate models based on data collected on the system. The proposed method allows to monitor the performance of damping controllers and even to perform redesign based on the models derived with system identification. The resulting redesign could be used to update PSS parameters and improve damping without the need of removing existing damping control systems from service.

Keywords: Power system monitoring, PSS redesign, system identification

1. Introduction

Power System Stabilizers (PSS) are a well established technology used to provide damping for electro-mechanical oscillations via a synchronous machine excitation control system (ECS) by placing the PSS in cascade with an

Automatic Voltage Regulator (AVR) [1]. It is to be noted that similar damping controllers are used in Flexible Alternating Current Transmission Systems (FACTS) [2, 3] and High-Voltage Direct Current (HVDC) links [4, 5, 6]. It is also to be noted that, with the increasing adoption and maturity of new measurement technologies, new damping control schemes leveraging real-time data have been proposed [7, 8, 9, 10, 11, 12]. While these new controllers might be suitable for new installations, in this paper, we will focus on conventional PSS controllers that are deployed in existing plants.

In the case of conventional PSS, to perform their damping function satisfactorily, their control parameters need to be adequately designed to provide damping over a range of different conditions and for different oscillatory modes (if required). This is typically carried out during a power plant commissioning, during scheduled maintenance or required tests [13, 14, 15], and involves an off-line design process using simulation models and an on-line re-calibration [14, 16]. Such process is obviously laborious, time consuming and requires specialized knowledge, and therefore, it is not carried out as regularly as needed[1]. Even with careful design and regular update of PSS parameters, under stringent operating conditions and the loss of important transmission corridors [17], the performance of the PSS may still degrade, without a possibility of quickly updating the design of each generator controller or other devices contributing to damping control [18, 19, 4], which weakens the system stability margins. This has led, for example, to major recent oscillatory incidents in Europe [20, 21, 22] and will continue to challenge its operation with additional expansions [19, 23], with a 2021 report from an European Expert Panel highlighting the importance of better assessment in operational planning and real-time operations for the critical transmission system corridors w.r.t. dynamic stability [22].

One of the major challenges with the physics-based model approach for PSS design is the dynamic model itself [24]. Adequate models are required for control design, and maintaining these models updated regularly is challenging even only at the plant level [25, 26], let alone for the entire power grid.

[1] A notable exception is the US Western Interconnection, which establishes performance criteria for PSS via standard VAR-501-WECC-3.1 and enforces requirements, see: *https://www.nerc.com/pa/Stand/Pages/VAR501WECC3.1RI.aspx*.

A continental European model only first become available in 2015 [27] and it is not used currently used in operational planning, let alone for PSS design. Meanwhile, the use of new measurement technologies has become advantageous in the development and application of real-time monitoring of different types of system dynamics [20, 28, 29, 30], to perform root-cause analysis of oscillatory issues both at the local level [31] and for wide-area oscillations [32].

These new measurement technologies enable system identification techniques [33] to derive simple and accurate models of power systems by injecting small "probing" signals at well chosen locations of the power system. As shown in [34, 35, 36], system identification has already been proven useful for the monitoring of the damping ability of the power system i.e., to verify whether this damping ability remains satisfactory at a given moment in time. The measurement-based model used to perform this monitoring is a model of the *closed-loop* system, i.e., the system with the dynamics of the PSS controller. In this paper, the main contribution is to show that, **if the probing signal is injected at the output of the PSS controller, we can not only identify a model of the closed-loop system** (allowing the monitoring of the damping ability of the current PSS controller), **but also derive, from this closed-loop model, a simple and accurate model of the open-loop system i.e., the system as seen by the PSS controller.** This property is crucial. Indeed, if the monitoring algorithm (which is based on the closed-loop model) detects a drop in the damping ability of the current PSS controller, it is necessary to redesign the PSS controller in order to increase its damping performance. This can only be done if an open-loop model is available. Note furthermore that, because the open-loop system may be unstable, identifying a model of this open-loop system is generally a difficult task that can be tackled elegantly using the approach proposed in this paper.

If the performance of the current PSS controller has dropped, the PSS controller can thus be redesigned based on the open-loop model derived from the identified closed-loop model. For this purpose, we can make use of the numerous model-based control design techniques existing in the literature[2] The current field practice for PSS design and tuning is based on classical

[2]It is to be noted that, as opposed to *model-based techniques*, the literature also proposes a number of fully data-driven techniques. See e.g., [37, 38].

control methods [39, 40]. Several sophisticated control design techniques have been discussed in the literature, some summarized in [1, 16]. See also [41, 42]. All these techniques could be used to redesign the PSS controller based on the open-loop model. In this paper, inspired by [41], we formulate the PSS redesign problem as an optimization problem. The advantage of this formulation is that it allows to maximize the damping while limiting control effort. Even though other techniques may also achieve the compromise between sufficient damping and acceptable control efforts (e.g., the one in [41]), to the author's knowledge, very little attention has been devoted in the literature to this important aspect of the PSS control problem. We show, in the numerical examples in this paper, that considering this aspect allows one to improve the PSS controller performance.

To sum up, this paper presents an integrated procedure, based on system identification techniques, to monitor the damping ability of a PSS controller and to redesign this PSS controller when its performance has dropped. In a power system, there may be several PSS controllers and retuning all of them may lead to coordination issues. To avoid this problem, we will here focus on the monitoring and the potential redesign of the PSS controller in one particular machine using measurements obtained at this machine (i.e., the other PSS controllers will not be re-tuned).

The reminder of this paper is organized as follows. In Section 2 the problem statement is delineated and notation is described. In Section 3 the methodology for data-driven PSS damping performance monitoring is outlined while in Section 4 the methodology for PSS redesign is described. Sections 5 and 6 present two proof-of-concept examples illustrating the proposed methodology. Finally, conclusions and future works are outlined in Section 7.

2. Problem Statement

In this paper, we consider a power plant equipped with a PSS damping controller and that is interconnected with a power grid. The PSS damping controller uses a measurement of the speed w of the rotor shaft of the power plant to compute a correction signal that is applied to the AVR control loop and that aims at increasing the damping of eventual electro-mechanical oscillations that could arise due to disturbances in the power network (see

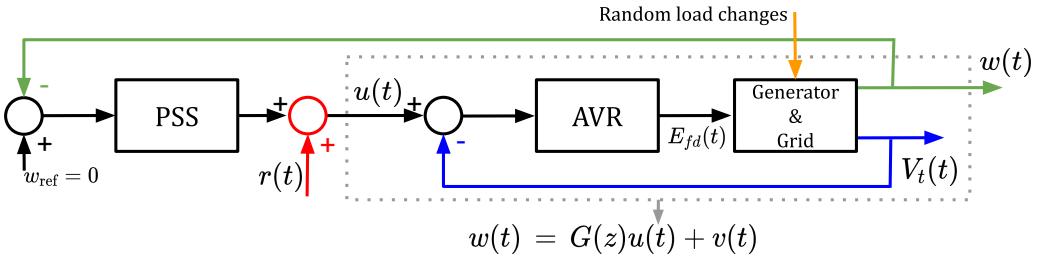

Figure 1: PSS control strategy in a power plant. The signal $v(t)$ represents the influence of the random load changes on $w(t)$. The probing signal $r(t)$ is equal to zero except during an identification experiment (see Section 3).

Figure 1). It is clear that such a controller is crucial to help maintain the stability of a power system. As already mentioned in the introduction, if we can assume that the PSS controller will achieve sufficient performance at its commissioning, it is not guaranteed that this performance can be maintained over time due to possible changes of the dynamics of the power plant and/or of the power network. Because these changes are nowadays more and more frequent, it is crucial, on the one hand, to have a methodology allowing a close monitoring of the PSS performance and, on the other hand, to have also a methodology allowing to redesign the PSS controller if the monitoring algorithm detects a drop in the PSS performance. In this paper, we propose a procedure that integrates two of such methodologies, and show that both objectives can be achieved using measurement data collected on the power system and with mathematical models derived/identified based on these data.

If we have a high-fidelity simulator of the power system (i.e., the power plant equipped with the PSS controller and the power grid to which this power plant is connected), the performance of the PSS controller can be evaluated by determining the damping of the poles of a linearized version of this power system and by checking that these dampings are all above a certain threshold. If such high-fidelity simulator is not available or no longer accurate due to changes in the power system, an alternative approach is to identify a linear model (i.e., a transfer function model) of the power system around its current operating condition and to subsequently compute the dampings of the poles of that model (which are estimates of the actual dampings). In order to identify this model, we can inject a small probing signal at a given location, measure its effect on a measured variable of the

power system and subsequently identify the *closed-loop* transfer function T_0 between the probing signal and this measured variable. Note that, in this approach, the obtained model will be an accurate representation of the current situation of the power system. This is an important advantage with respect to the approach based on an high-fidelity simulator whose accuracy can be deteriorated due to changes in either the power plant or the power grid. Consequently, this data-driven approach is particularly interesting for the monitoring of the PSS performance. Indeed, if we perform this identification at a regular basis, we can monitor this performance by verifying that the minimal damping of the poles of the identified model $\hat{T}$ of T_0 remain above a certain threshold.

For monitoring purposes, the measured variable mentioned in the previous paragraph and the location at which the probing signal is injected can be chosen in a rather arbitrary way. In this paper, we will inject the probing signal at the output of the PSS controller and choose the rotor shaft speed w as the measured variable (see Figure 1). These choices have indeed the advantage that the identified model $\hat{T}$ between this probing signal and w can be used to derive a model $\hat{G}$ of the *open-loop* system between the output of the PSS controller and the rotor shaft speed w (i.e. the open-loop system that the PSS controller regulates). This model $\hat{G}$ is indeed crucial to be able to redesign the PSS controller whenever the performance of the current PSS controller will be deemed too low by the monitoring algorithm. Since $\hat{G}$ will be deduced from the identified model $\hat{T}$, the whole procedure for PSS monitoring and redesign can be implemented using solely measurement data collected on the power system and the probing signal.

Notations. We will denote continuous-time signals as $x(t)$ with $t \in \mathbf{R}$ and continuous-time transfer functions as $H(s)$ with s representing both the Laplace variable and the derivation operator. We can thus write $y(t) = H(s)u(t)$ for the linear relation between a continuous-time input signal $u(t)$ and a continuous-time output signal $y(t)$. Discrete-time signals will be denoted as $x[n]$ with n an integer. If $x[n]$ is the sampled version of $x(t)$, we have that $x[n] \stackrel{\Delta}{=} x(t = nT_s)$ with T_s the sampling time. Discrete-time transfer functions will be denoted as $H(z)$ with z representing both the Z-transform variable and the shift operator. Consequently, we can write $y[n] = H(z)u[n]$ for the linear relation between a discrete-time input signal $u[n]$ and a discrete-

time output signal $y[n]$.

3. PSS Performance Monitoring: a data-driven monitoring algorithm exploiting probing

In this section, we present the data-driven approach to evaluate the performance of the current PSS controller. Because the dynamics of the power system may change over time, the procedure described in this section must thus be repeated at regular basis.

Let us first say a few words about how we can model the power system based on data. From the point-of-view of the PSS controller and assuming that the power system is operating around an equilibrium, we can use the following linear representation of the power system (see also Figure 1):

$$w(t) = G_0(s)u(t) + v(t) \tag{1}$$

$$u(t) = -K(s)w(t) \tag{2}$$

where $K(s)$ is the continuous-time transfer function of the PSS controller, $w(t)$ is the rotor shaft speed, $u(t)$ is the output of the PSS controller and $v(t)$ represents the stochastic disturbance acting on the system due to random load changes[3]. In (1), $G_0(s)$ represents the dynamics of the power system between $u(t)$ and $w(t)$ and therefore embeds the dynamics of the AVR, of the generator and of the power grid to which the generator is connected. Since we assume that the power system is operating around an equilibrium, we can therefore assume that these dynamics can be represented by a linear transfer function $G_0(s)$.

The system (1)-(2) is a so-called closed-loop system for which we will use the shorthand notation $[K(s)\ G_0(s)]$. The performance of the PSS controller $K(s)$ is generally deemed satisfactory if the dampings of the poles of this closed-loop system are all larger than a certain threshold β (say $\beta = 12\%$).

[3]Since (1)-(2) is a representation of the power system around an equilibrium, these signals in fact represent the deviations of the signals with respect to the setpoint.

The poles of the closed-loop system (1)-(2) can be determined by computing the poles of any[4] of the four so-called closed-loop transfer functions:

$$\frac{1}{1+K(s)G_0(s)},\ \frac{K(s)}{1+K(s)G_0(s)},\ \frac{G_0(s)}{1+K(s)G_0(s)}\ \text{and}\ \frac{K(s)G_0(s)}{1+K(s)G_0(s)}. \quad (3)$$

Let us introduce some notations for further reference. For any given K and G, the minimal damping of the poles of the closed-loop system $[K\ G]$ will be denoted by $\xi_{min}(K,G)$. If T denotes one of the four closed-loop transfer functions of $[K\ G]$, we will also use the notation $\xi_{min}(T)$ for the same quantity i.e., $\xi_{min}(T) = \xi_{min}(K,G)$. We will use these notations for continuous-time and for discrete-time transfer functions K, G and T, assuming that the sampling time T_s has been chosen appropriately so that, e.g., $\xi_{min}(T(z)) = \xi_{min}(T(s))$ when $T(z)$ is the discrete-time version of $T(s)$.

Using these notations, the performance of the PSS controller $K(s)$ will be deemed satifactory whenever the following condition holds:

$$\xi_{min}(K(s), G_0(s)) > \beta \quad (4)$$

If the controller $K(s)$ can be assumed fully known, the open-loop system $G_0(s)$ is of course unknown[5]. Consequently, to be able to evaluate the PSS performance, we will need to identify a model of G_0 or a model of one of the four closed-loop transfer functions (3) in order to be able to check (4). Since G_0 may be unstable in some cases and since the identification of stable transfer functions are easier in practice, we have here decided to identify a model of one of the stable closed-loop transfer functions (3), in particular:

$$T_0(s) = \frac{G_0(s)}{1+K(s)G_0(s)} \quad (5)$$

Let us describe the experiment we will devise to collect the data that are required for the identification of a model of T_0: we will excite the closed-loop system (1)-(2) with a small probing sign $r(t)$ at the output of the PSS

[4]If we assume that the product $K(s)G_0(s)$ happens without pole-zero cancellation, these four closed-loop transfer functions have indeed the same poles.

[5]As mentioned in Section 2, the system $G_0(s)$ can also change over time. We will however suppose that $G_0(s)$ will remain constant during the identification experiment described in this section.

controller (see Figure 1). This small probing signal can be chosen as a white noise or as a sum of sinusoids at different frequencies (i.e., a multisine). During the identification experiment, (1)-(2) therefore becomes:

$$w(t) = G_0(s)u(t) + v(t) \tag{6}$$

$$u(t) = -K(s)w(t) + r(t) \tag{7}$$

Note that (6)-(7) can be rewritten in the following closed-loop form:

$$w(t) = T_0(s)\ r(t) + \underbrace{\frac{1}{1 + K(s)G_0(s)} v(t)}_{v_{cl}(t)} \tag{8}$$

where the signal $v_{cl}(t)$ (which is a function of $v(t)$ as shown in (8)) is also a stochastic disturbance that can be assumed to be statistically independent from the probing signal $r(t)$. Using (8), we observe that, if we identify the transfer function between the known excitation signal $r(t)$ and the measurable signal $w(t)$, we will obtain a model of the closed-loop transfer function $T_0(s)$ (from which we will be able to assess the damping ability of the PSS controller).

For this purpose, we can use the so-called prediction-error identification methodology [33] that uses discrete-time data collected on the system (6)-(7) with a sampling time T_s:

$$Z^N = \{w[n],\ r[n] \mid n = 1, ..., N\} \tag{9}$$

where N represents the number of collected data (NT_s is the duration of experiment). Due to (8), the input-output data in Z^N can be related as follows:

$$w[n] = T_0(z)\ r[n] + H_0(z)\ e[n] \tag{10}$$

with $T_0(z)$ the discrete-time version of $T_0(s)$, $e[n]$ a zero-mean white noise, and $H_0(z)$ a monic transfer function guaranteeing that the time-series $H(z, \theta_0)\ e[n]$ has the same power spectrum as the discrete-time version of $v_{cl}(t)$.

In the prediction error identification framework, we also need to define a so-called model structure $\mathcal{M} = \{T(z, \theta),\ H(z, \theta) \mid \theta \in \mathbf{R}^k\}$ i.e., a

parametrization for the to-be identified models of $T_0(z)$ and $H_0(z)$ (θ is the parameter vector gathering the k coefficients of the numerators and denominators of $T(z,\theta)$ and $H(z,\theta)$). Based on the data set Z^N and the chosen model structure $\mathcal{M}$, the optimal parameter vector $\hat{\theta}_N$ can be deduced as follows [33]:

$$\hat{\theta}_N = \arg\min_{\theta} \frac{1}{N} \sum_{n=1}^{N} \epsilon^2[n,\theta] \tag{11}$$

$$\epsilon[n,\theta] = H^{-1}(z,\theta) \ \left(w[n] - T(z,\theta)r[n]\right). \tag{12}$$

In general, the order of the parametrized transfer functions $T(z,\theta)$ and $H(z,\theta)$ in $\mathcal{M}$ are chosen in such a way that the prediction error $\epsilon[n,\hat{\theta}_N]$ is close enough to a white noise [33]. If that is the case, we can say that the model structure $\mathcal{M}$ is full-order and that $\hat{\theta}_N$ is a consistent estimate of the so-called unknown true parameter vector θ_0 i.e., the parameter vector such that $T(z,\theta_0) = T_0(z)$ and $H(z,\theta_0) = H_0(z)$. In this case, we can also assess the modeling error $\hat{\theta}_N - \theta_0$. Indeed, it is shown in [33] that $\hat{\theta}_N$ is (asymptotically) normally distributed around the true parameter vector θ_0 and with a covariance matrix P_θ that can be estimated using $\hat{\theta}_N$ and Z^N [33]. Using this statistical property, we can derive an ellipsoid $U_{\hat{\theta}_N}$ centered at $\hat{\theta}_N$ and containing, at a certain probability level, the true parameter vector θ_0. The size of this uncertainty ellipsoid $U_{\hat{\theta}_N}$ is directly related to the covariance matrix P_θ and will decrease if the number of data N increases (P_θ indeed converges to zero when $N \to \infty$) [33].

Let us now come back to our problem of evaluating the PSS performance, which boils down to verifying that (4) holds. Note also that $\xi_{min}(K(s), G_0(s))$ is by definition equal to $\xi_{min}(T_0(s)) = \xi_{min}(T_0(z))$. Now, recall that, using the data Z^N and the criterion (11), we obtain a model $T(z,\hat{\theta}_N)$ for the unknown closed-loop transfer function T_0. Consequently, we have that $\xi_{min}(T(z,\hat{\theta}_N))$ is an estimate for $\xi_{min}(T_0(z))$ and we can verify whether the PSS performance is satisfactory by checking whether:

$$\xi_{min}(T(z,\hat{\theta}_N)) > \beta. \tag{13}$$

A finer condition to check the PSS performance can be deduced by making use of the parametric uncertainty ellipsoid $U_{\hat{\theta}_N}$. Let us for this purpose derive, based on $U_{\hat{\theta}_N}$, an uncertainty interval $\mathcal{I}$ for the unknown $\xi_{min}(T_0(z)) =$

$\xi_{min}(T_0(s))$:

$$\mathcal{I} = \{\xi_{min}(T(z,\theta)) \mid \theta \in U_{\hat{\theta}_N}\}. \tag{14}$$

It is clear that, if θ_0 lies in $U_{\hat{\theta}_N}$, $\xi_{min}(T_0(z)) = \xi_{min}(T(z,\theta_0))$ also lies in $\mathcal{I}$. Assuming that this is the case, (4) holds if all elements ξ of $\mathcal{I}$ are larger than β i.e.,

$$\xi > \beta \quad \forall \xi \in \mathcal{I}. \tag{15}$$

If the latter condition is verified, we have then a strong indication that the PSS performance remains satisfactory and no action will be undertaken. In the opposite case, we will need to update the PSS controller to restore the performance. The procedure for this purpose will be detailed in the next section.

Remark. In order to verify (15), we need an explicit expression of the interval $\mathcal{I}$ (the definition (14) for $\mathcal{I}$ is indeed implicit). Due to nonlinear relation between θ and $\xi_{min}(T(z,\theta))$, an exact explicit description for this interval is not available. However, $\mathcal{I}$ can be easily approximated using a gridding approach (i.e., by generating a number of grid points θ_i in $U_{\hat{\theta}_N}$ and by computing $\xi_{min}(T(z,\theta_i))$ for all these grid points θ_i). Another approach based on a linearization of the relation between θ and $\xi_{min}(T(z,\theta))$ is given in [43, 36].

4. Redesign: PSS controller update in case when its performance is deemed unsatisfactory

As mentioned above, if (15) is not verified, the damping $\xi_{min}(T_0) = \xi_{min}(K, G_0)$ is likely to be too low to guarantee sufficient damping of the power system when major disturbances arise. Consequently, the PSS controller $K(s)$ needs to be updated in order to restore the desired damping performance. This will be achieved by replacing the original controller $K(s)$ in (1)-(2) by a new controller $K_{new}(s)$.

Because of the complex dynamics of the open-loop system $G_0(s)$ (e.g., it may be unstable in some cases), we will require a model of $G_0(s)$ in order to redesign the PSS controller. This model of G_0 will be derived from the model $T(z,\hat{\theta}_N)$ of the closed-loop transfer function $T_0(s)$ that has been identified in

the monitoring procedure. For this purpose, let us observe that:

$$T_0(s) = \frac{G_0(s)}{1 + K(s)G_0(s)} \Longrightarrow G_0(s) = \frac{T_0(s)}{1 - K(s)T_0(s)} \tag{16}$$

Using this relation and the fact that $T(z, \hat{\theta}_N)$ is a model of $T_0(s)$, we can derive the following discrete-time model $G(z, \hat{\theta}_N)$ of the unknown continuous-time system $G_0(s)$:

$$G(z, \hat{\theta}_N) = \frac{T(z, \hat{\theta}_N)}{1 - K(z)T(z, \hat{\theta}_N)} \tag{17}$$

where $K(z)$ is the discrete-time version of the original controller $K(s)$. Note that we use the expression of the original controller K in (16) and in (17) since $T(z, \hat{\theta}_N)$ has been identified based on data collected on the power system operated with this original controller (see (6)-(7)).

As usual in the model-based control design paradigm, the controller K_{new} will be synthetised in such a way that K_{new} achieves the desired control objective when applied to the model $G(z, \hat{\theta}_N)$ of G_0. Denoting $K_{new}(z)$ the discrete-time version of $K_{new}(s)$, the main control objective is of course to have the largest possible value for $\xi_{min}(K_{new}(z), G(z, \hat{\theta}_N))$. However, if considered alone, this objective may lead to overly large control signals $u[n] = -K_{new}(z)w[n]$. Consequently, the objective of maximizing $\xi_{min}(K_{new}(z), G(z, \hat{\theta}_N))$ must be balanced by the objective of having a control action that remains limited. In the H_∞ control design framework [44], this can be achieved by constraining the H_∞-norm of the closed-loop transfer function $\frac{K_{new}(z)}{1+K_{new}(z)G(z,\hat{\theta}_N)}$. In the same H_∞ control framework, a good practice (in order to ensure the robustness of the controller with respect to the uncertainty of the model) is also to limit the H_∞-norm of the closed-loop transfer function $\frac{1}{1+K_{new}(z)G(z,\hat{\theta}_N)}$ (the so-called sensitivity function) to be less[6] than 2 [44].

This leads to the following model-based control design problem whose solution is the controller $K_{new}(z)$:

$$\arg \max_{\tilde{K}} \ \xi_{min}(\tilde{K}(z), G(z, \hat{\theta}_N)) \tag{18}$$

[6]Other weightings can also be considered to further shape the sensitivity function [44].

$$\text{subject to } \left\| \begin{pmatrix} \frac{0.5}{1+\tilde{K}(z)\ G(z,\hat{\theta})} \\ \frac{\gamma\ \tilde{K}(z)}{1+\tilde{K}(z)\ G(z,\hat{\theta})} \end{pmatrix} \right\|_\infty < 1 \tag{19}$$

where $\tilde{K}(z)$ is the decision variable of the optimization problem (18)-(19) and γ is a tuning parameter that is chosen in order to limit the control action in a satisfactory manner. Note that (19) implies that[7] the solution K_{new} of (18)-(19) satisfies:

$$\left\| \frac{1}{1+K_{new}(z)\ G(z,\hat{\theta})} \right\|_\infty < 2 \ \text{ and } \ \left\| \frac{K_{new}(z)}{1+K_{new}(z)\ G(z,\hat{\theta})} \right\|_\infty < \frac{1}{\gamma} \tag{20}$$

From this expression, it is clear that the larger γ, the less aggressive the control action will be. The optimization problem (18)-(19) can be solved for different values of γ to see how large γ can be chosen while guaranteeing a sufficient value of the damping.

Such control design formulation is relatively classical in H_∞ control [45, 41]. In practice, if the structure of the PSS controller would have not be constrained, the optimization problem (18)-(19) could have been solved elegantly using LMI optimization. However, in many cases, the structure of the PSS controller ($K(s)$ and $K_{new}(s)$) is constrained to be a washout filter or a washout filter followed by two lead-lag filters[8]. In other words, the decision variable $\tilde{K}(s)$ in the optimization problem (18)-(19) is constrained to have one of the following two structures:

$$\tilde{K}(s) = k_w\ \frac{t_w\ s}{1+t_w\ s} \tag{21}$$

$$\tilde{K}(s) = k_w\ \frac{t_w\ s}{1+t_w\ s}\ \frac{1+t_1\ s}{1+t_2\ s}\ \frac{1+t_3\ s}{1+t_4\ s} \tag{22}$$

Due to this fixed structure, redesigning the PSS controller (i.e., determining $K_{new}(s)$) boils down to retuning the values of the coefficients in the considered

[7] In the H_∞ framework, the constraint (19) is generally more complex. However, finer weighting is not necessary in this case because sufficient shaping of $1/(1+K_{new}(z)\ G(z,\hat{\theta}))$ is indirectly imposed by the objective of maximal damping.

[8] Note that other fixed controller structures could also be similarly considered.

structure i.e., retuning k_w and t_w for (21) or k_w, t_w, t_1, t_2, t_3 and t_4 for (22). In the numerical illustrations (see Sections 5 and 6), we will see that a washout filter structure (21) will generally be sufficient to achieve sufficient damping performance[9]. An important consequence of the fixed controller structure is that the optimization problem (18)-(19) becomes non-linear. There are different ways to tackle this non-linear optimization problem. Here, since the number of controller parameters to be determined in K_{new} is limited, we will use Bayesian optimization which somehow implements a smart gridding process by modeling both the objective function and the constraint of (18)-(19) as a so-called Gaussian process (see [46]).

The (fixed structure) controller K_{new} is thus the solution of the optimization problem (18)-(19). The minimal damping of the closed loop $[K_{new}(z)\ G(z,\hat{\theta}_N)]$ is by definition equal to $\xi_{min}(K_{new}(z), G(z,\hat{\theta}_N))$. Before applying the updated controller K_{new} to the power system (and forms in this way the closed-loop system $[K_{new}\ G_0]$ having a minimal damping $\xi_{min}(K_{new}, G_0)$), a first verification consists in checking that $\xi_{min}(K_{new}(z), G(z,\hat{\theta}_N)) > \beta$. Similarly as in Section 3, it is also good practice to determine an uncertainty interval $\mathcal{I}_{new}$ for $\xi_{min}(K_{new}, G_0)$:

$$\mathcal{I}_{new} = \left\{ \xi_{min}(K_{new}(z), G(z,\theta)) \mid G(z,\theta) = \frac{T(z,\theta)}{1 - K(z)T(z,\theta)} \ \text{ and } \ \theta \in U_{\hat{\theta}_N} \right\} \tag{23}$$

and by checking that all elements of $\mathcal{I}_{new}$ are larger than β. This uncertainty interval $\mathcal{I}_{new}$ can here also be approximated using a gridding approach.

When the above verifications are completed, the new PSS controller can be implemented and we can return to the monitoring mode. An additional verification can be carried out by performing the identification procedure of the previous section on the updated closed-loop system to verify that the PSS performance has indeed be restored.

[9] If the controller structure is (22), a washout filter can be obtained by putting $t_1 = t_2 = t_3 = t_4 = 0$.

5. First Case study

5.1. Scenario

5.1.1. Considered power system model

In order to provide a proof-of-concept of the integrated monitoring and redesign procedure, we have developed a power system simulation model that we will use as true real-life system. More precisely, we consider the power system represented in Figure 2. Recall that, by power system, we here mean the interconnection of the power grid and of the power plant whose PSS controller has to be monitored. In Figure 2, the power plant is represented by $G1$ and the power grid to which it is connected consists in four buses ($B1$, $B2$, $B3$ and $B4$), four lines ($L1$, $L2$, $L3$, and $L4$), a load (*Load* in Figure 2) and a block *Grid* that represents the reminder of the power grid and that is here modeled using an Infinite Bus [39]. The power plant $G1$ is here chosen as a synchronous generator controlled as shown in Figure 1 with an AVR controller and a PSS controller. The modeling details will be given in the next subsection.

In normal operation (i.e., when there is no identification experiment being conducted), this power system will be entirely driven by the so-called random load changes i.e., the variation of the load *Load* with respect to its steady state value. These random load changes will be here modeled as a zero-mean Gaussian white noise e_{load} with standard deviation 0.0577 (see Figure 2). Note that this white noise is the phenomenon causing the stochastic disturbance v in (1).

As we will see in the sequel, in order to assess the damping ability of the PSS controller, we will need to be able to subject the power system to a large disturbance. In order to simulate such a large disturbance, we will suppose that the variation of the load with respect to its steady state value is the sum of the Gaussian white noise e_{load} (of relatively small amplitude) and of a large pulse signal p_{load} (see block `Pulse` in Figure 2). Finally, when an identification experiment is performed (see Section 3), a probing signal r must be added at the output of the PSS controller (see Figure 1). This probing signal r and the load changes e_{load} and p_{load} will be the sole exogenous inputs of the power system simulation model considered in this case study; they are therefore represented at the bottom of Figure 2 (see the hatched red box).

In the considered power system simulator, the to-be-monitored PSS controller has the form of a washout filter and has been pre-designed as:

$$K(s) = k_w \frac{t_w\ s}{t_w\ s + 1} \quad \text{with } k_w = 9.5 \text{ and } t_w = 1.41 \tag{24}$$

By linearizing[10] between r and w the power plant simulation model with the PSS controller (24), we determine the closed-loop transfer function T_0 and we observe that $\xi_{min}(T_0) = 16.84\%$. Note that this minimal damping of 16.84% corresponds to a complex pole at a frequency of 10.6 rad/s ($\approx 1.69\ Hz$). Since $\xi_{min}(T_0) = 16.84\%$ is larger than $\beta = 12\%$, the PSS controller achieves satisfactory performance in this initial situation.

A dynamical change is introduced to this power system by removing Line $L4$ (i.e., this line is tripped). By linearizing the power plant simulation model between r and w in this new situation, we obtain a new closed-loop transfer function T_0 and we observe that the critical mode has now a much lower damping of $\xi_{min}(T_0) = 7.08\%$ at a frequency of 6.5 rad/s ($\approx 1\ Hz$). This damping $\xi_{min}(T_0) = 7.08\%$ is now (much) smaller than $\beta = 12\%$ i.e., the PSS performance is no longer satisfactory. We will see that this performance drop can be detected using our identification-based monitoring procedure (see Section 3) and a new PSS controller can be designed using the procedure presented in Section 4.

For the identification of the model $T(z, \hat{\theta}_N)$ of T_0 in the monitoring procedure (see Section 3), we will apply, for a duration of twenty minutes, a multisine probing signal $r(t)$ given by:

$$r(t) = A \sum_{k=1}^{50} sin(\omega_k t + \phi_k) \tag{25}$$

with $A = 1.1 \times 10^{-3}$, random phase shifts ϕ_k ($k = 1, ..., 50$) and $\omega_k = \frac{k}{2}\ rad/s$ ($k = 1, ..., 50$) (the frequencies ω_k thus range from 0.5 rad/s till 25 rad/s). For the chosen random phase shifts ϕ_k ($k = 1, ..., 50$), the maximal amplitude of this multisine $r(t)$ is 0.016. As we will see in the next subsection, the perturbation induced by this probing signal will be completely acceptable.

[10] This linearization is performed according to the approach described in [47].

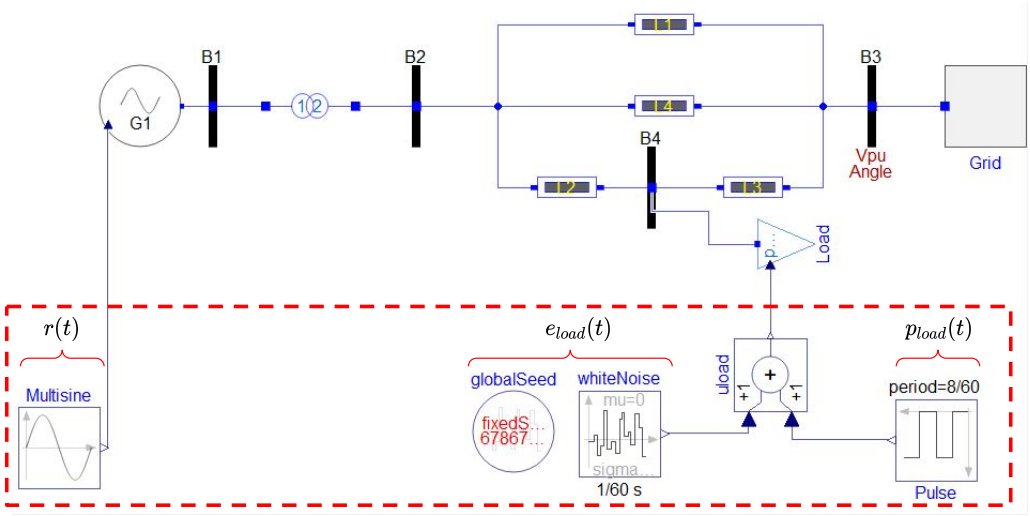

Figure 2: Power system simulation model developed using Modelica and the OpenIPSL library with exogenous inputs e_{load}, p_{load} and r.

5.1.2. Modeling details

Following well established approaches [48], the power system simulator described in the previous subsection is developed with the Modelica language *https://modelica.org/*, the Modelica Standard Library (MSL) *https://doc.modelica.org/*, the Open-Instance Power Systems Library (OpenIPSL) [49], and assembled using the Dymola software *http://dymola.com/*. All OpenIPSL models used to develop the system models in this paper are open-source software and can be found online at *https://openipsl.org*. In the sequel, when referring to the model components in these figures, we will use the `typewriter` font and the Modelica dot notation.

Let us first describe the power plant (denoted $G1$ in Figure 2) in more details. The power plant model $G1$ is given in Figure 3 and contains the two control loops depicted in Figure 1. As shown in Figure 3, $G1$ contains a synchronous machine represented using a 6-th order model (`PSAT.Order6` from OpenIPSL), an excitation control system (that includes the AVR) represented with the `PST.AVRtypeIII` model, and a single-input PSS controller modeled with the `PSAT.PSSTypeII`. Note that both the excitation control system and the PSS controller have limiters enabled. Note also that the PSS model `PSAT.PSSTypeII` includes three transfer functions in cascade: a

washout filter with gain $k_w \times t_w$ and time constant t_w, and two lead-lag compensators, with gains K, T_1 and T_2, each (see Figure 4). Note that by setting $T_1 = T_2 = 0$ and $K = 1$, the PSS controller has the form (24).

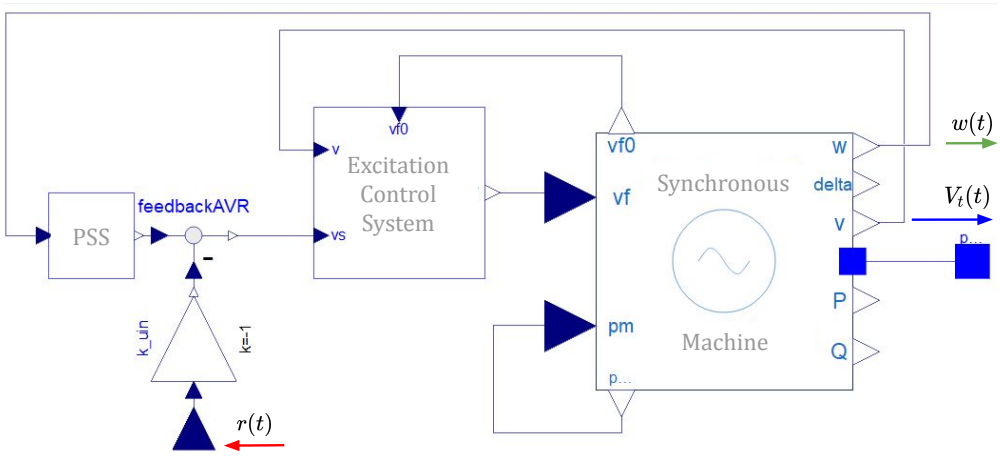

Figure 3: Power plant model inside of $G1$ in Figure 2 developed using Modelica and components from the OpenIPSL library. The probing input $r(t)$ is indicated with a red arrow and the signals $V_t(t)$ and $w(t)$ used in the two control loops of Figure 1 are represented with a blue and a green arrow, respectively (the signals r and w will also be used to identify the model $T(z, \hat{\theta}_N)$ of T_0).

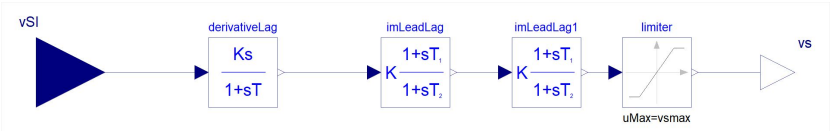

Figure 4: Inside the PSS `PST.PSSTypeII` component model.

The complete simulation models can be found online at *https://github.com/ALSETLab/PSSMonitoringAndRedesign*.

We can run simulations on that simulation model by applying the exogenous inputs described in the previous subsection. Note that the simulations will all be performed with a variable integration step, but all the signals will nevertheless be re-sampled to have a fixed sampling time of $1/60$ s.

Let us say a few words on how the exogenous inputs are applied to the simulation model. As mentioned in the previous subsection, the random load

changes are modeled by a zero-mean Gaussian white noise e_{load} with standard deviation 0.0577. This white noise is generated by the block `whiteNoise` in Figure 2 with a sample time of $1/60$ s. The component, `globalSeed` in the same figure specifies a fixed number for initialization of a pseudo random number generator. The value is constant to keep the same noise for all simulations, as recommended in [50].

As already mentioned in the previous subsection, the large pulse disturbance p_{load} will be generated via the block `Pulse` in Figure 2. In this block, we can specify the amplitude and the duration of p_{load}.

The probing signal $r(t)$ defined in (25) is applied to the output of the PSS controller via the component `Multisine` (see Figure 3). Within this component, as shown in Figure 5, the signal r is in fact represented by a time vs. data table (see the `MultisineData` component, which is a `CombiTimeTable` block from the MSL). This allows to keep the definition of the probing signal generic. Observe that, in Figure 5, there are also other blocks that help to define when r is applied and when it is set to zero.

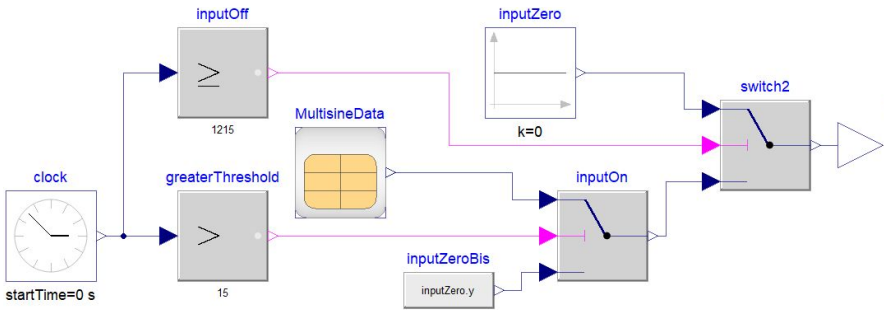

Figure 5: Inside the `Multisine` component model.

Before illustrating the methodologies introduced in Sections 3 and 4 on this power system simulation model, let us present an example of possible simulations. In this example, the simulation scenario follows a sequence of actions:

A. at $t = 0$ s, initialization and start of the simulation,

B. at $t = 0.1$ s, the Gaussian withe noise e_{load} (i.e., the stochastic load) starts driving the system and stays present throughout the simulation

until $t = 1245\ s$,

C. at $t = 0.5\ s$, Line 4 is removed/tripped (the dynamics of the power system change),

D. at $t = 15\ s$, the probing noise $r(t)$ (see (25)) is applied until $t = 1215\ s$, corresponding to 20 minutes of probing,

E. at $t = 1215\ s$, $r(t) = 0$ until $t = 1245\ s$,

Note that p_{load} is set to zero throughout this simulation. In the left column of Figure 6, we represent, from $t = 0$ to $t = 1245\ s$, the signals V_t (plot (a)) and w (plot (b)) obtained via this simulation as well as the exogenous inputs r (plot (c)) and e_{load} (plot (d)) (a zoom on the particular time interval [0 45] s is given in the right column). As mentioned in Section 5.1.1, we observe in plot (c) that the maximal amplitude of the probing signal r is indeed equal to 0.016.

The combined effect of r and e_{load} on the internal variables V_t and w can be observed in plots (a) and (b) in the time interval [15 1215] s while the effect of only e_{load} can be observed in the same plots in the time interval [1215 1245] s. In these plots, we observe that the perturbation induced by the probing signal is, as indicated at the end of the previous subsection, completely acceptable: the maximal excursions of the signals V_t and w around their steady state are indeed respectively equal to 0.02 $p.u.$ and 0.002 rad/s, which are very small values. Note that the control signals u and E_{fd} also never hit their limits when the probing signal is added.

In plots (e) and (f) of Figure 6, we can observe the long transient of the system dynamics after the tripping of line $L4$ (occurring at $t = 0.5\ s$). This long transient of about 10 seconds is consistent with the fact that the PSS controller K given in (24) only achieves a very small damping of 7.08% in this new situation (see Subsection 5.1.1) and also confirms that, in this new situation, the damping ability of the PSS controller (24) is no longer satisfactory.

Note finally that the transient mentioned above has disappeared before the application of the probing signal (i.e., at $t = 15\ s$). Consequently, if the data set Z^N (see (9)) is collected from $t = 15\ s$ till $t = 1215\ s$, these data will be representative of the power system with line $L4$ removed.

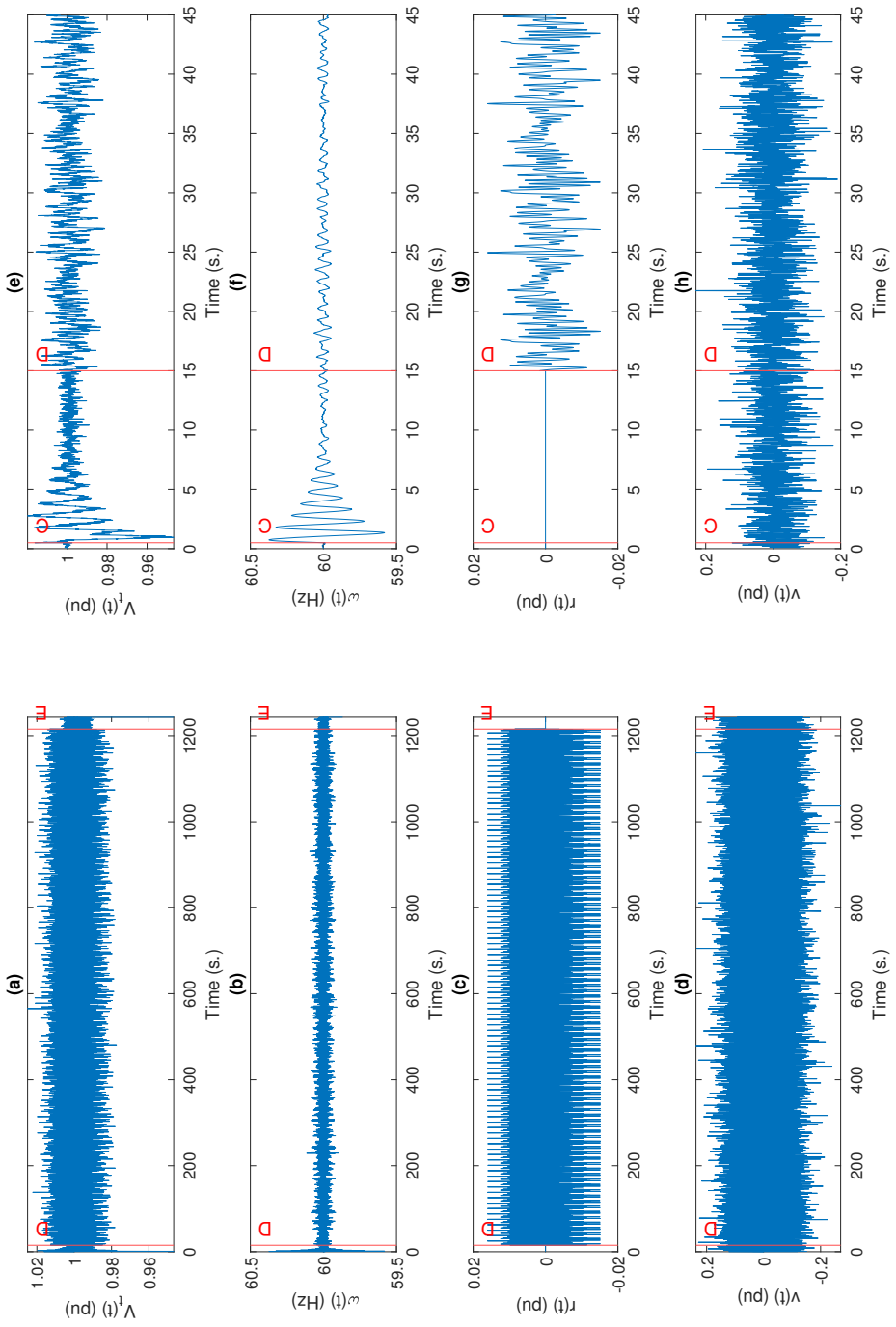

Figure 6: Nonlinear simulation results. Left column, time period $t = [0 - 1245]$ s, right column $t = [0 - 45]$ s. Vertical red lines indicate a specific actions from the list in Section 5.1.2.

5.2. Monitoring

In Section 5.1.1, via linearization between r and w of the power system simulation model with line $L4$ removed, we have obtained the closed-loop transfer function T_0. The modulus of the frequency response of this transfer function is represented in Figure 7 (dashed blue curve). This transfer function T_0 is characterized by $\xi_{min}(T_0) = 7.08\%$ (the small damping of T_0 is also evidenced by the sharp peak around 6.5 rad/s (≈ 1 Hz) in Figure 7). Since $\xi_{min}(T_0) = 7.08\%$ is smaller than $\beta = 12\%$, (4) does not hold.

Let us see whether we can detect this problem using the identification procedure of Section 3. For this purpose, we will use prediction error identification to obtain a (discrete-time) model $T(z, \hat{\theta}_N)$ of T_0. In order to identify the model $T(z, \hat{\theta}_N)$, we need to collect the data set (9). For this purpose, we will apply the probing signal r defined in (25) during twenty minutes[11] on the power system simulation model with the tripped line $L4$ and we will collect the corresponding output signal w. As mentioned at the end of Section 5.1.2, these data can e.g. be the data collected between $t = 15$ s and $t = 1215$ s in the simulation of Figure 6. In this simulation, the data are collected with a sampling rate of 60 samples per second. In order to avoid the numerical errors inherent to discrete-time transfer functions with a sampling rate that is too large with respect to their main dynamics, we decimate these data with a factor 3 yielding a sampling rate of 20 samples per second (or $T_s = 0.05$ s). This corresponds to a Nyquist frequency of 10 Hz (or 63 rad/s) which is approximately one decade above the main dynamics of T_0 (see Figure 7).

The obtained data set Z^N (see (9)) is thus characterized by $N = 24000$. Using an ARMAX model structure $\mathcal{M}$ of order 4, the data set Z^N and the criterion (11), we determine an optimal parameter vector $\hat{\theta}_N$ that yields a nearly[12] white prediction error $\epsilon[n, \hat{\theta}_N]$. This identification procedure thus yields a fourth order model $T(z, \hat{\theta})$:

$$T(z, \hat{\theta}_N) = \frac{0.001353 + 0.000571\ z^{-1} + 0.003511\ z^{-2} - 0.005439\ z^{-3}}{1 - 2.3\ z^{-1} + 1.964\ z^{-2} - 0.7605\ z^{-3} + 0.1719\ z^{-4}}$$

[11] We will analyze the impact of a smaller probing duration at the end of this section.

[12] Even though one of the residual tests on $\epsilon[n, \hat{\theta}_N]$ [33, page 511] is not fully satisfied, this fourth order ARMAX model structure seems acceptable. Indeed, increasing the order or using a Box-Jenkins model structure do not improve this residual test.

and, since $\epsilon[n, \hat{\theta}_N]$ is almost white, we can also determine the parametric uncertainty ellipsoid $U_{\hat{\theta}_N}$.

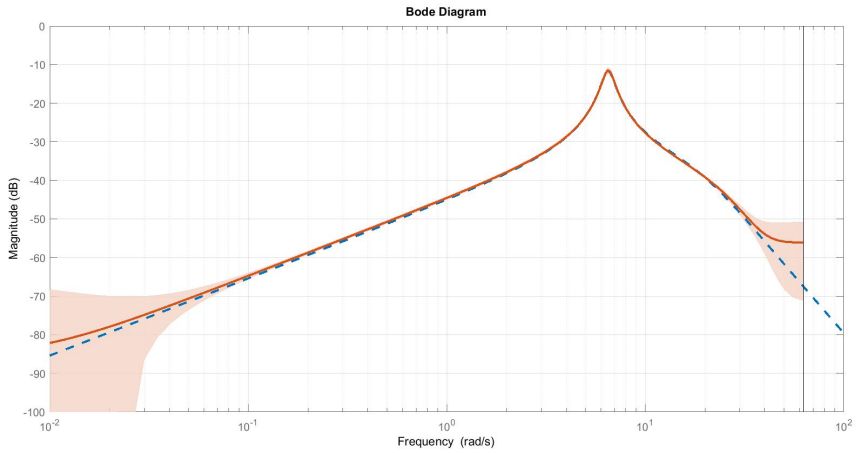

Figure 7: Magnitude plot of $T_0(s)$ (blue dashed) and of $T(z, \hat{\theta})$ (red solid). The shaded area around $|T(e^{j\omega T_s}, \hat{\theta}_N)|$ is the projection in the frequency domain of the parametric uncertainty region $U_{\hat{\theta}_N}$.

In Figure 7, we compare the modulus of the frequency response of $T(z, \hat{\theta})$ with the one of $T_0(s)$ and we observe that $T(z, \hat{\theta})$ is a close estimate[13] of T_0. In this figure, we also represent with the shaded area the uncertainty of the identified model in the frequency domain (obtained by projecting the parametric uncertainty ellipsoid $U_{\hat{\theta}_N}$ in the frequency domain) and we see that the uncertainty is very small in the frequency band of interest.

Let us now use $T(z, \hat{\theta}_N)$ to compute the estimate $\xi_{min}(T(z, \hat{\theta}_N))$ of $\xi_{min}(K, G_0) = 7.08\%$ as well as the uncertainty interval[14] $\mathcal{I}$ (see (14)). We obtain $\xi_{min}(T(z, \hat{\theta}_N)) = 6.97\%$ and the uncertainty interval $\mathcal{I}$ is given by [6.41 7.53] % (using the approach in [43, 36]) and by [6.54 7.41] % (using the gridding approach with

[13]Note that the transfer function $T_0(s)$ obtained via linearization of the power system simulation model is a transfer function of order 12, but, as shown in Figure 7, this transfer function can relatively be well approximated by the fourth order transfer function $T(z, \hat{\theta}_N)$.

[14]Using the insights in [51], we here determine the size of $U_{\hat{\theta}_N}$ to guarantee that $\mathcal{I}$ is a 99%-confidence interval.

1000 randomly chosen grid points in $U_{\hat{\theta}_N}$). We observe that $\xi_{min}(T(z,\hat{\theta}_N)) = 6.97\%$ is a close estimate of $\xi_{min}(K,G_0) = 7.08\%$ and that $\xi_{min}(K,G_0) = 7.08\%$ lies in the uncertainty intervals obtained using both approaches. It is also clear that (15) is not satisfied and thus the identification procedure allows to detect that the PSS performance has been degraded due to the loss of the line. We therefore decide to redesign the PSS controller.

Before redesigning the PSS, let us first analyze the influence of the experiment duration on the above result. If we reduce the experiment duration to 10 minutes (resp. 5 minutes), we obtain as expected a larger uncertainty interval $\mathcal{I} = [6.20\ 7.81]$ % (resp. $\mathcal{I} = [6.07\ 8.44]$ %). Both intervals are computed using the approach in [43, 36]. However, the alteration of PSS performance can be still detected since (15) remains not satisfied in both situations.

5.3. PSS controller redesign

5.3.1. Redesign

We have thus detected that the original controller $K(s)$ leads to a degraded performance with a damping $\xi_{min}(K,G_0) = 7.08\%$ which is much too low. We therefore apply the procedure described in Section 4 to obtain a new PSS controller K_{new} with an acceptable performance. We will assume that this new controller has the same structure as the original controller[15]:

$$K_{new}(s) = k_{w,new}\frac{t_{w,new}\ s}{t_{w,new}\ s+1} \tag{26}$$

Following the procedure in Section 4, we first compute $G(z,\hat{\theta}_N)$ using (17) and the model $T(z,\hat{\theta}_N)$ identified using the experiment of 20 minutes[16]. In order to analyze the effect of the tuning parameter γ, we solve the optimization problem (18)-(19) with $\gamma = 0.025$ and with $\gamma = 0.05$. The controller $K_{new,1}$ obtained with $\gamma = 0.025$ is characterized by $k_{w,new} = 22.4455$ and $t_{w,new} = 0.5217$. The (in theory less aggressive) controller $K_{new,2}$ obtained with $\gamma = 0.05$ is characterized by $k_{w,new} = 12.6924$ and $t_{w,new} = 0.5602$.

[15]This simple structure is here not a limitation. In order to verify that, we have also solved the (convex) optimization problem (18)-(19) in the case where no particular controller structure is imposed and we have not observed a better performance than the one obtained with the washout filter structure.

[16]In this case, the obtained model $G(z,\hat{\theta})$ happens to be unstable.

In Figure 8, $K_{new,1}(s)$ and $K_{new,2}(s)$ are compared to the original controller $K(s)$.

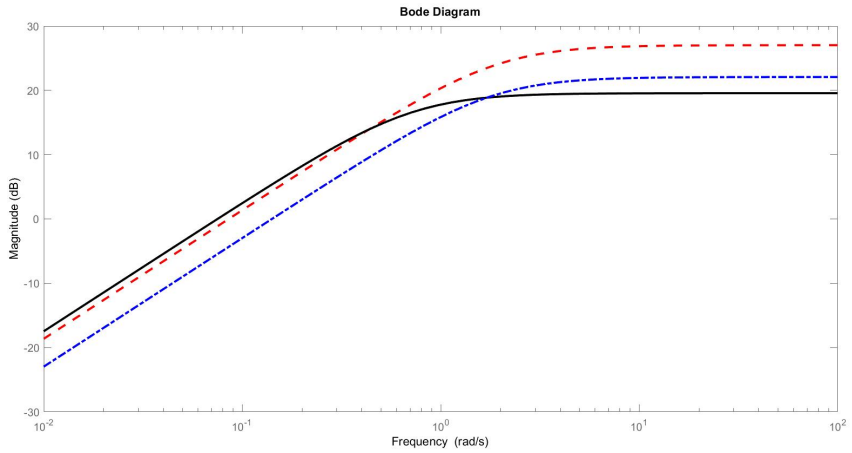

Figure 8: Magnitude plot of $K(s)$ (black solid), of $K_{new,1}(s)$ (red dashed) and of $K_{new,2}(s)$ (blue dash-dotted).

Since the constraint (19) in the optimization problem yielding $K_{new,1}(s)$ is less stringent, the obtained damping $\xi_{min}(K_{new,1}, G(z, \hat{\theta}_N)) = 38.51\%$ is higher than the one obtained with $K_{new,2}(s)$ i.e., $\xi_{min}(K_{new,2}, G(z, \hat{\theta}_N)) = 13.54\%$. The uncertainty intervals $\mathcal{I}_{new}$ are respectively $\mathcal{I}_{new} = [36.83\ 40.05]$ % for $K_{new,1}(s)$ and $\mathcal{I}_{new} = [12.95\ 14.15]$ % for $K_{new,2}(s)$. Since the elements of these two intervals are all above $\beta = 12\%$, those two controllers can be implemented on the power system in lieu of the original controller $K(s)$. The above analysis indeed indicates that they could strongly improve the PSS performance.

5.3.2. Verification of the performance of $K_{new,1}(s)$ and $K_{new,2}(s)$ using linear analysis on the power system simulation model

We have thus implemented those two controllers on the power system simulation model. Let us denote by $T_{0,new,1}(s)$ (resp. $T_{0,new,2}(s)$) the linearization of the dynamics between r and w of the power system simulation model when $K_{new,1}(s)$ (resp. $K_{new,2}(s)$) is implemented as the PSS controller. The modulus of the frequency response of these two closed-loop

transfer functions is represented in Figure 9 and compared with the modulus of the closed-loop transfer function T_0 corresponding to the original controller $K(s)$ (see (24)). We directly observe the less sharper peak in $T_{0,new,1}(s)$ and $T_{0,new,2}(s)$ indicating a larger damping. More precisely, with $K_{new,1}(s)$, we obtain $\xi_{min}(T_{0,new,1}) = 39.26\%$ while, with $K_{new,2}(s)$, we obtain $\xi_{min}(T_{0,new,2}) = 13.78\%$. This is entirely in accordance with the predictions that have been made on the basis of the model $G(z, \hat{\theta}_N)$ at the end of the previous subsection and we also observe that 39.26 % (resp. 13.78%) lies in the uncertainty interval $\mathcal{I}_{new}$ corresponding to $K_{new,1}(s)$ (resp. $K_{new,2}(s)$).

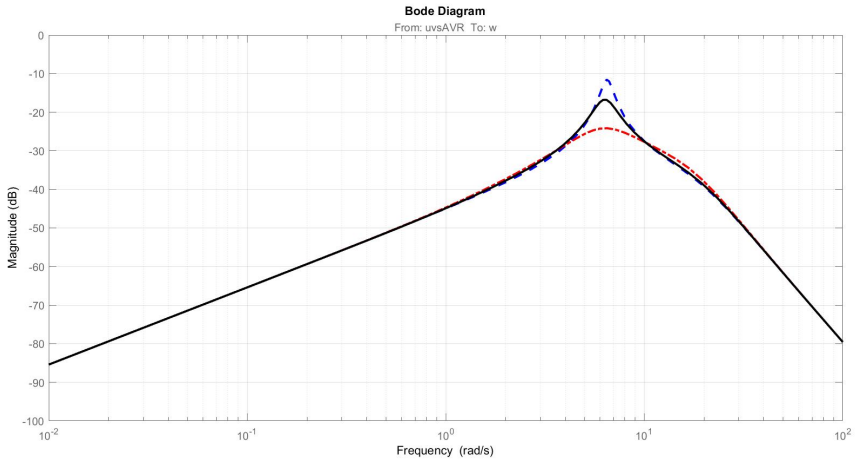

Figure 9: Magnitude plot of $T_0(s)$ (blue dashed) of $T_{0,new,1}(s)$ (red dashdotted) and of $T_{0,new,2}(s)$ (black solid)

An identification experiment on the updated power system simulation model with the same multisine probing signal $r(t)$ as in Section 5.2 yields a model $T(z, \hat{\theta}_N)$ with a minimal damping of 36% when $K_{new,1}(s)$ is implemented as the PSS controller. A similar experiment yields a model $T(z, \hat{\theta}_N)$ with a minimal damping of 13.52% when $K_{new,2}(s)$ is implemented. As expected, such identification experiments could therefore confirm that these two PSS controllers achieve satisfactory performance.

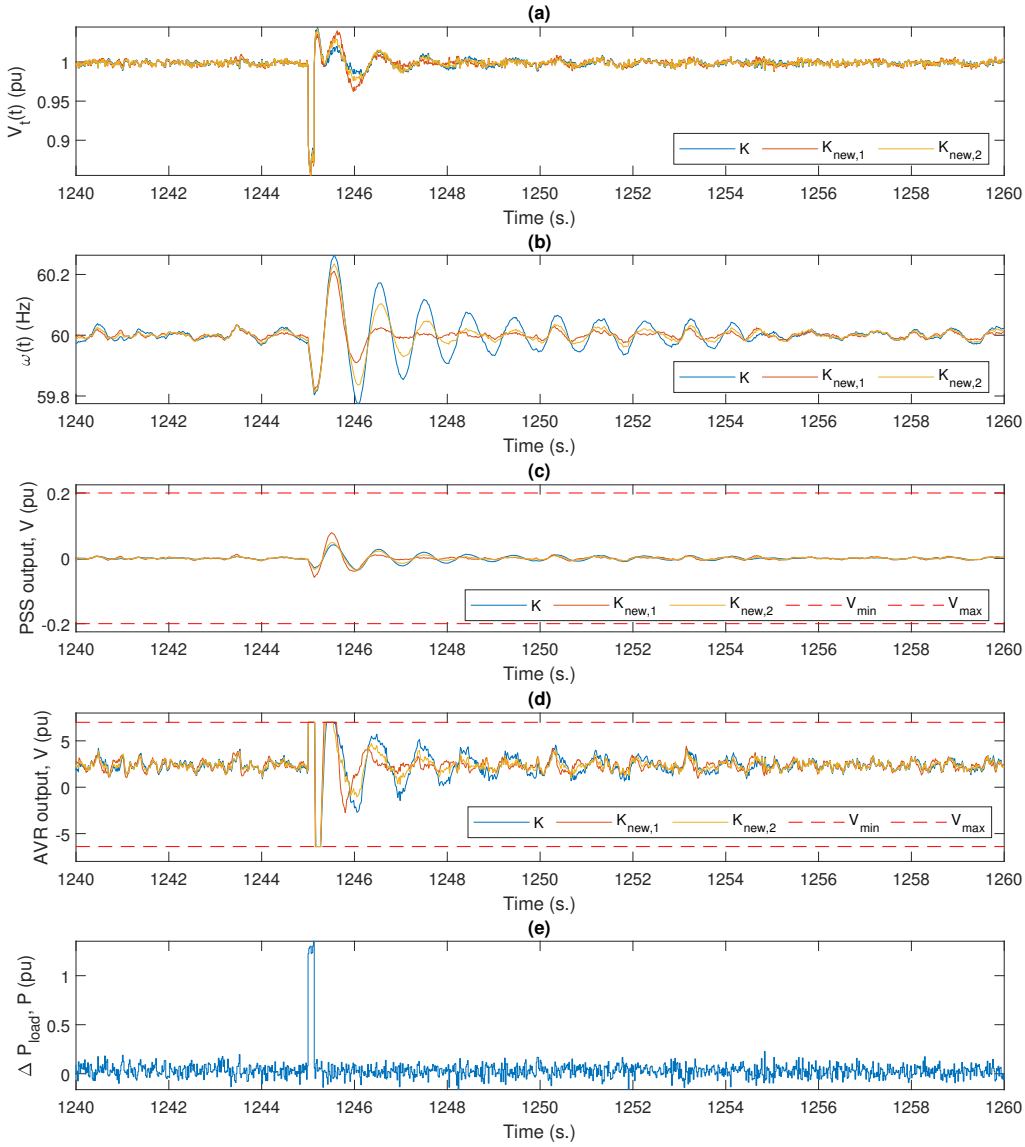

Figure 10: Performance of $K(s)$ (blue), $K_{new,1}(s)$ (orange) and $K_{new,2}(s)$ (yellow) under a large load disturbance p_{load} of amplitude 1.25 $p.u.$ and with a duration of 8 cycles.

5.3.3. Verification of the performance of $K_{new,1}(s)$ and $K_{new,2}(s)$ for large load disturbance on the power system simulation model

The linear analysis performed in the previous section seems to indicate that $K_{new,1}(s)$ and $K_{new,2}(s)$ will show better damping ability than the original controller $K(s)$ when the power system is subject to a large disturbance. We will now verify this in practice on the nonlinear power system simulation model. We will for this purpose make use of the block `Pulse` in Figure 2. Recall that this block allows to add, to the random load change e_{load}, a pulse signal p_{load}. The amplitude and the duration of p_{load} will be here first fixed respectively to 1.25 $p.u.$ (125 MW) and to eight cycles (i.e., 8/60 s). It is clear that such a p_{load} can be considered as a massive load disturbance.

In order to evaluate the performance of the controllers $K(s)$, $K_{new,1}(s)$ and $K_{new,2}(s)$ under this massive load disturbance, we have performed a simulation on the power system simulation model when each of these threes controllers are implemented as the PSS controller. In this simulation, the probing signal r is set to zero, the Gaussian white noise e_{load} is applied during the whole simulation and the large pulse disturbance p_{load} is applied at $t = 1245$ s. The modification of the load with respect to its set-point is thus given by plot (e) in Figure 10. In the same figure, we compare the terminal voltage $V_t(t)$ (plot (a)), the rotor shaft speed $w(t)$ (plot (b)), the control action $u(t)$ (plot (c)) and the field voltage $E_{fd}(t)$ (plot (d)) obtained in the simulations with the three different controllers $K(s)$, $K_{new,1}(s)$ and $K_{new,2}(s)$. Note that, in plots (c) and (d), the horizontal dashed red lines correspond to the min. and max. voltage limits of the PSS controller (generating $u(t)$) and of the AVR controller (generating $E_{fd}(t)$).

In these plots, we clearly see that the three controllers lead to a stable behaviour under this massive disturbance. However, as can be seen in plot (b), the transient behaviour is strongly reduced by replacing the original controller $K(s)$ by the new controllers. With $K(s)$, we indeed observe a transient of about 10 seconds[17], while the transient only lasts 2 seconds with $K_{new,1}(s)$ and 4 seconds with $K_{new,2}(s)$. This confirms the improved damping performance expected from Section 5.3.1.

[17] A similar transient has also been observed in plot (f) of Figure 6.

It is important to note that the less aggressive new controller $K_{new,2}(s)$ achieves this reduced damping with control efforts that are similar to (in fact, even slightly smaller than) the one with the original controller $K(s)$ (see plots (c) and (d) in Figure 10). As expected, the controller $K_{new,1}(s)$ (achieving very high damping) goes hand in hand with (slightly) larger control efforts. It is however to be noted that these (slightly) larger control efforts are only observed for approximately one second after the application of p_{load}. After this initial second, the control efforts with $K_{new,1}(s)$ and $K_{new,2}(s)$ become similar.

From these plots, it also clear that, for $K_{new,1}(s)$ and $K_{new,2}(s)$, the PSS output $u(t)$ never reaches its limit, while the limit for E_{fd} is only hit during the on-set of the large disturbance p_{load} (i.e., for about 0.5 s). Note that this seems unavoidable for such a drastic load change p_{load} and that this is also the case for the original controller K.

Let us now perform the same analysis with a pulse of even higher amplitude (i.e., 1.3275 $p.u.$) and a (much) larger duration of 22 cycles. With this even more massive load disturbance, we perform the same simulation as above (the only difference is that e_{load} is set to zero to make the plots clearer). This leads to Figure 11 that has the same structure as Figure 10. In this figure, we clearly see that the original controller $K(s)$ destabilizes the power system. When analyzing the blue line in plot (b), it is indeed obvious that the machine looses synchronism shortly after $t \approx 1248$ s. This is a direct result of the PSS output $u(t)$ reaching its maximum voltage limit at this moment (as shown in plot (c)). Meanwhile, in plot (d), it can also be observed how the AVR is fighting to stabilize the machine during the transient but its response is bounded by its limit even before $t = 1248$ s. In contrast, we observe how $K_{new,1}$ and $K_{new,2}$ are able to keep the system stable (see orange and yellow curves in plots (a)-(d)). Similarly as what was the case in Figure 10, the transient is shorter with $K_{new,1}$ (see plot (b)) and, during the first second after the application of p_{load}, $K_{new,1}$ leads to a larger $u(t)$ than $K_{new,2}(s)$ (see plot (c)). However, as shown in plot (d), the field voltage E_{fd} with $K_{new,1}$ makes first its return to a region within the limits. Regardless, both controllers can effectively stabilize the power system for this disturbance p_{load} of amplitude 1.3275 $p.u.$ and of duration equal to 22 cycles while it is not the case with the original PSS controller.

Note that the original controller $K(s)$ still stabilizes the power system when a pulse of amplitude 1.3275 $p.u.$ and of duration equal to 21 cycles is applied. In other words, for a pulse load disturbance of amplitude 1.327 $p.u.$, 21 cycles is the longest duration before destabilization for the original controller $K(s)$. With $K_{new,2}$, we can go to 24 cycles before destabilization and, with the controller $K_{new,1}$ achieving the highest damping, we can even go to 26 cycles before destabilization. Consequently, $K_{new,1}(s)$ and $K_{new,2}(s)$ can effectively stabilize the system for a longer period than the original PSS design, which implies that the stability region for the system has been expanded with $K_{new,1}(s)$ and $K_{new,2}(s)$. The stability analysis discussed above is summarized in Table 1 and is illustrated in Figures 12 and 13 where we see the performance of the controllers $K_{new,1}(s)$ and $K_{new,2}(s)$ for pulses having the duration given in Table 1 and a duration just slightly larger. Figures 12 and 13 have the same structure as Figure 11 and are obtained using a similar simulation (i.e., e_{load} is set to zero and the pulse p_{load} is applied at $t = 1245\ s$).

PSS controller	Maximal duration (in cycles) before destabilization
$K(s)$	21
$K_{new,1}$	26
$K_{new,2}$	24

Table 1: Stability analysis for the PSS controllers $K(s)$, $K_{new,1}(s)$ and $K_{new,2}(s)$ for a pulse disturbance p_{load} of amplitude 1.3275 $p.u.$

From the analysis in this subsection, we can thus conclude that the controllers $K_{new,1}(s)$ and $K_{new,2}(s)$ strongly improve the performance with respect to the controller $K(s)$, validating in this way the procedure proposed in Sections 3 and 4 for the monitoring and the redesign of the PSS controller.

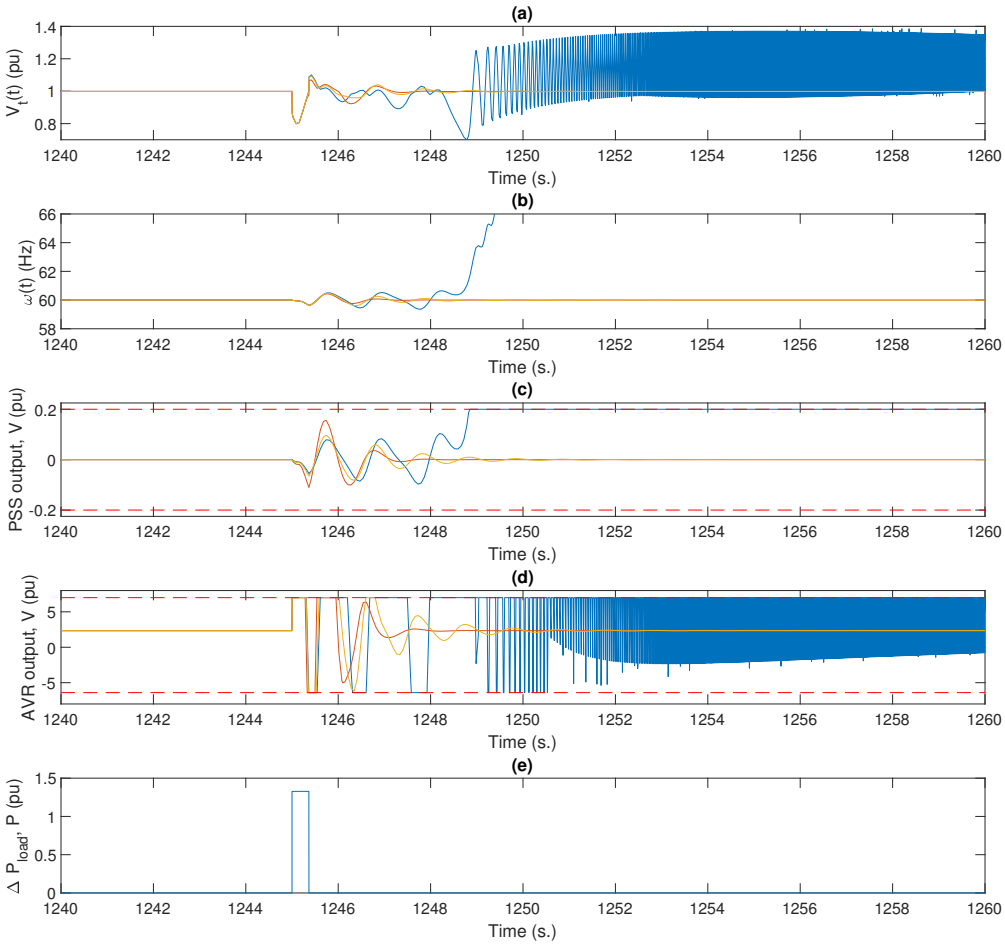

Figure 11: Performance of $K(s)$ (blue), $K_{new,1}(s)$ (orange) and $K_{new,2}(s)$ (yellow) under a large load disturbance p_{load} of amplitude 1.3275 $p.u.$ and with a duration of 22 cycles.

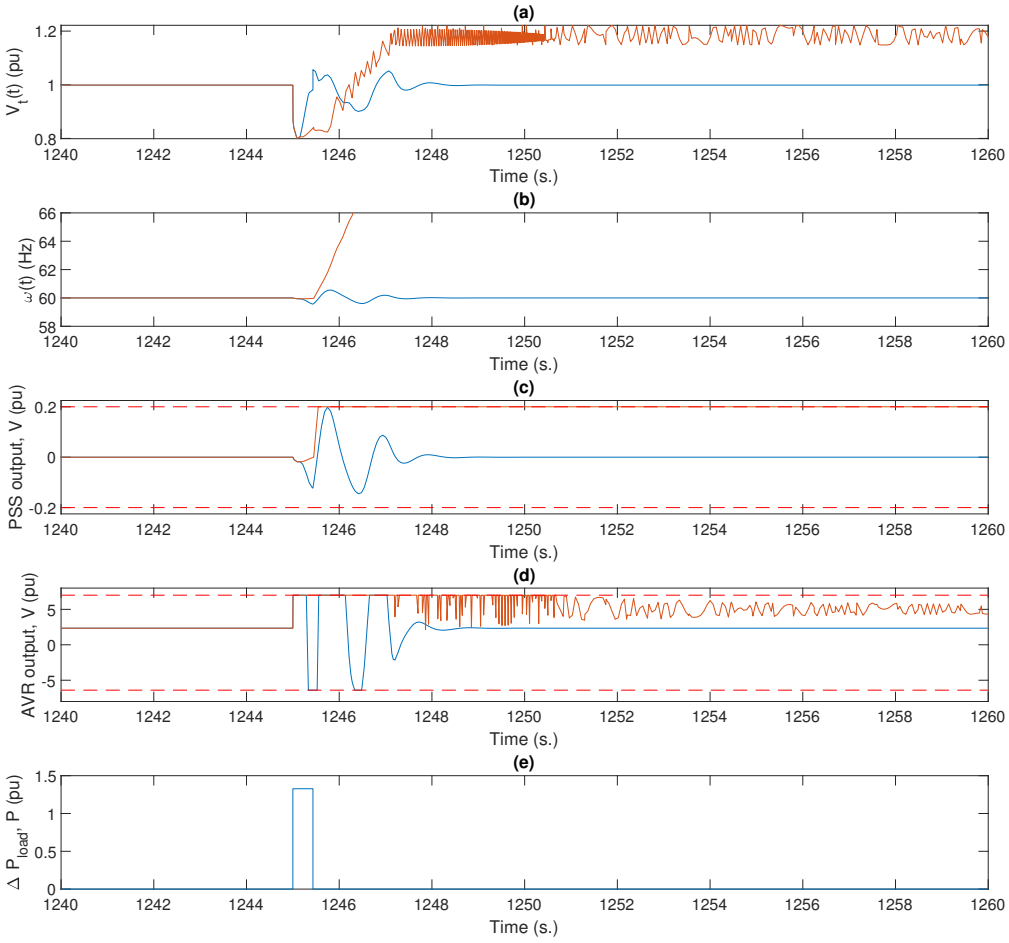

Figure 12: Performance of $K_{new,1}(s)$ for a pulse disturbance p_{load} of amplitude 1.3275 $p.u.$ and with a duration of 26 cycles (blue) and of 27 cycles (orange).

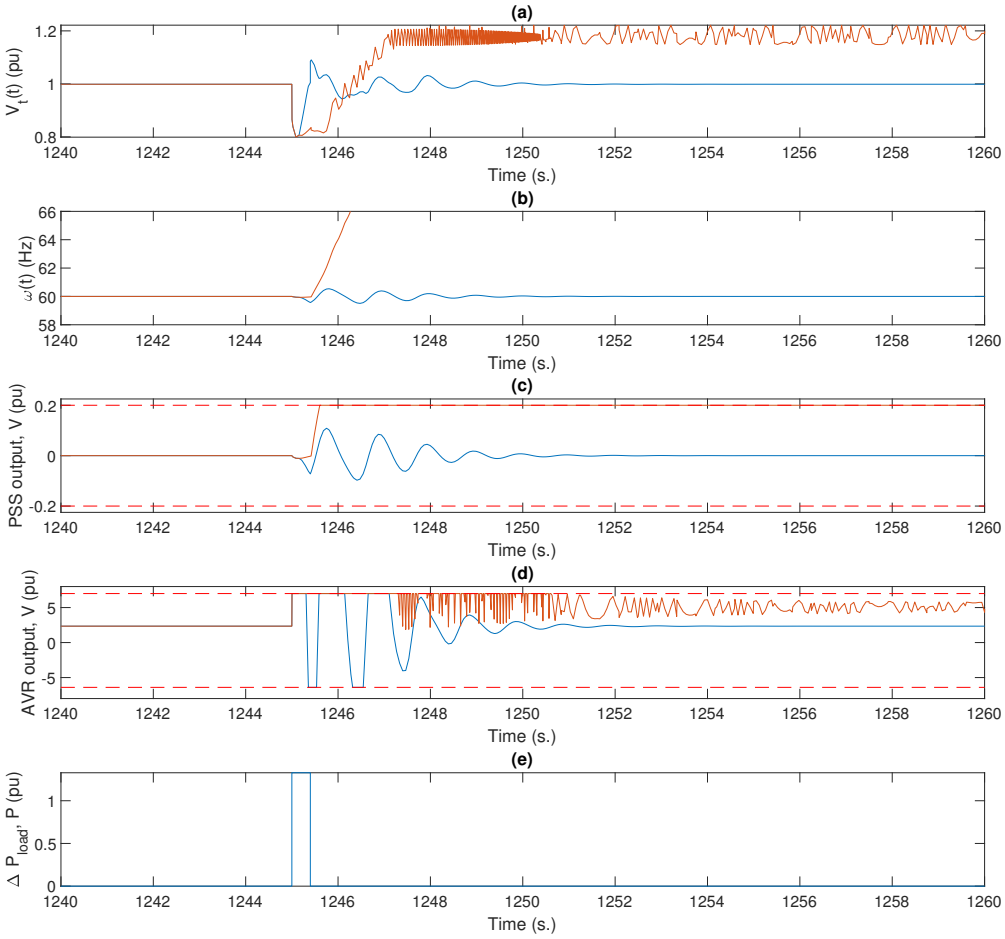

Figure 13: Performance of $K_{new,2}(s)$ for a pulse disturbance p_{load} of amplitude 1.3275 $p.u.$ and with a duration of 24 cycles (blue) and of 25 cycles (orange).

6. Second Case study

6.1. Considered power system

We now consider a more complex power system i.e., the classical two-area four-machine Klein-Rogers-Kundur (hereafter *Kundur*) system [52]. The complete simulation model corresponding to this second case study can also be found online. It is indeed distributed with the OpenIPSL library under `OpenIPSL.Examples.TwoAreas.Two_Areas_PSSE`.

In this simulation model, one of this machine (i.e., the generator connected to Bus 1, hereafter machine 1) is equipped with a PSS controller aiming at controlling both the inter-area mode and the local mode[18] between machine 1 and machine 2. Even though a simple wash-out filter could also be used (see later), this PSS controller has the following expression:

$$K(s) = 200 \ \frac{10 \ s}{10 \ s + 1} \ \frac{1 + 0.05 \ s}{1 + 0.02 \ s} \ \frac{1 + 3 \ s}{1 + 5.4 \ s} \tag{27}$$

This controller has thus the structure (22) and its parameters are taken from the design performed in [52]. The simulation model has otherwise the same features as the one in Section 5: it is possible to inject an excitation $r(t)$ at the output of the PSS controller, the system is subject to random load changes e_{load} and an additional large disturbance p_{load} can also be applied to test the performance of the PSS controller.

Using linearization techniques, we can deduce that the controller (27) achieves a minimal damping of around 30%. This minimal damping corresponds to the inter-area mode which is here characterized by a frequency of 4 rad/s (i.e., 0.6 Hz). A dynamical change is introduced to the Kundur system by removing a line (i.e., a line is tripped). This does not introduce any significant drop of performance: the minimal damping remains equal to 30.9 %.

6.2. Monitoring

Let us see whether this (maintained) performance can be detected using our identification procedure of Section 3. We therefore inject for twenty minutes a multisine $r(t)$ of maximal amplitude 0.013 at the output of the

[18] The local mode between machine 3 and machine 4 cannot be observed at machine 1.

PSS controller of machine 1 and we collect the speed w of machine 1. The simulation is here also run with a sampling rate of 60 Hz and the data are here also decimated with a factor three to avoid numerical errors.

The obtained data set Z^N (see (9)) is thus characterized by $N = 24000$. Using a BJ model structure, the data set Z^N and the criterion (11), we determine an eight-order model $T(z, \hat{\theta}_N)$ of the closed-loop system T_0 which has here an order of 27. This closed-loop system T_0 can be obtained by linearizing the power plant simulation model between r and w. In Figure 14, we show that, even though $T(z, \hat{\theta}_N)$ is of much lower order than T_0, $T(z, \hat{\theta}_N)$ is an accurate representation of the true transfer function T_0 (in the important frequency range). Even though the prediction error $\epsilon[n, \hat{\theta}_N]$ cannot be made completely white[19], we will nevertheless consider in the sequel the parametric uncertainty ellipsoid $U_{\hat{\theta}_N}$.

Let us now use $T(z, \hat{\theta}_N)$ to compute the estimate $\xi_{min}(T(z, \hat{\theta}_N))$ of $\xi_{min}(T_0) = 30.9\%$ as well as the uncertainty interval $\mathcal{I}$ (see (14)). We obtain $\xi_{min}(T(z, \hat{\theta}_N)) = 30\%$ and the uncertainty interval $\mathcal{I}$ is given by [29.21 30.88] % (using the gridding approach with 1000 randomly chosen grid points in $U_{\hat{\theta}_N}$). We observe that $\xi_{min}(T(z, \hat{\theta}_N)) = 30\%$ is a close estimate of $\xi_{min}(T_0) = 30.9\%$ and that $\xi_{min}(T_0) = 30.9\%$ almost lies in the uncertainty interval $\mathcal{I}$.

We thus observe that (15) is here satisfied and thus the identification procedure allows to determine that the PSS performance has not been degraded due to the loss of the line. In this case, according to the proposed methodology, the PSS controller does not need to be redesigned. However, we will nevertheless show that the open-loop model $G(z, \hat{\theta}_N)$ (that can be derived from $T(z, \hat{\theta}_N)$) allows one to reduce the control efforts without (significantly) reducing the damping ability.

6.3. PSS controller redesign

In order to do that, we first compute the open-loop model $G(z, \hat{\theta}_N)$ using (17) and the model $T(z, \hat{\theta}_N)$. Let us observe that the obtained open-loop

[19] In this example, the order of the identified model has been chosen to eight since, in this case, $\hat{w}[n] = T(z, \hat{\theta}_N)r[n]$ is very close to $w[n]$ (the so-called FIT to data [33] is equal to 95%).

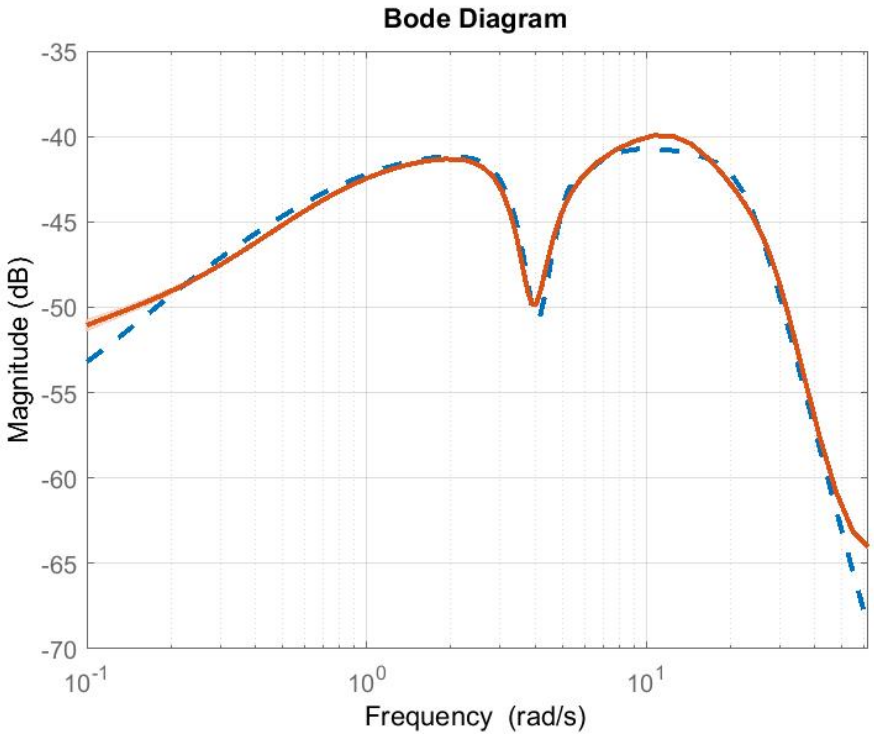

Figure 14: Magnitude plot of $T_0(s)$ (blue dashed) and of $T(z, \hat{\theta}_N)$ (red solid). The shaded area around $|T(e^{j\omega T_s}, \hat{\theta}_N)|$ is the projection in the frequency domain of the parametric uncertainty region $U_{\hat{\theta}_N}$.

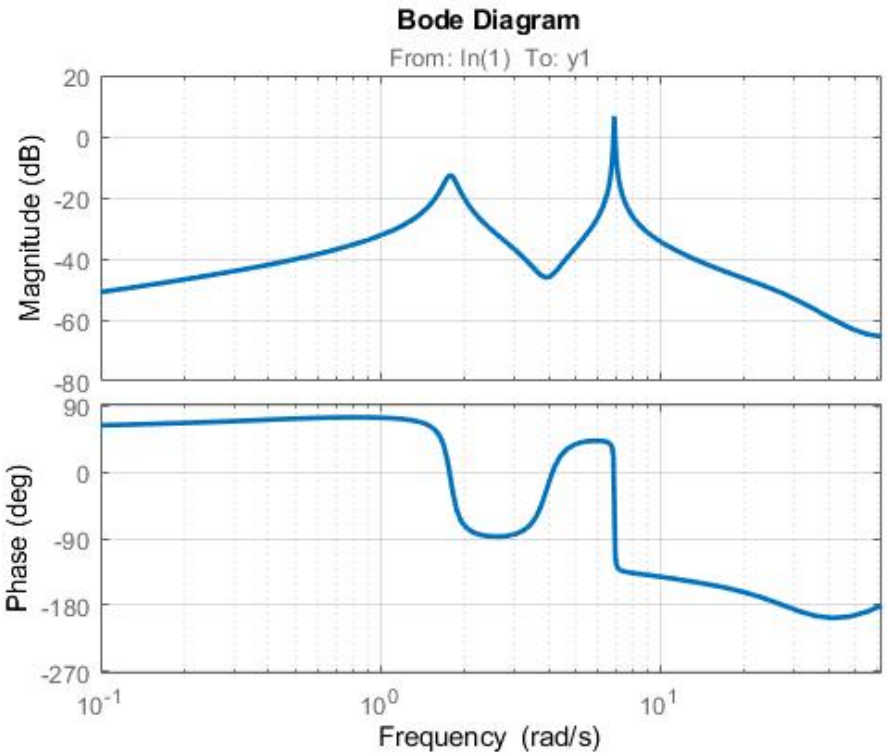

Figure 15: Bode diagram of $G(z, \hat{\theta}_N)$

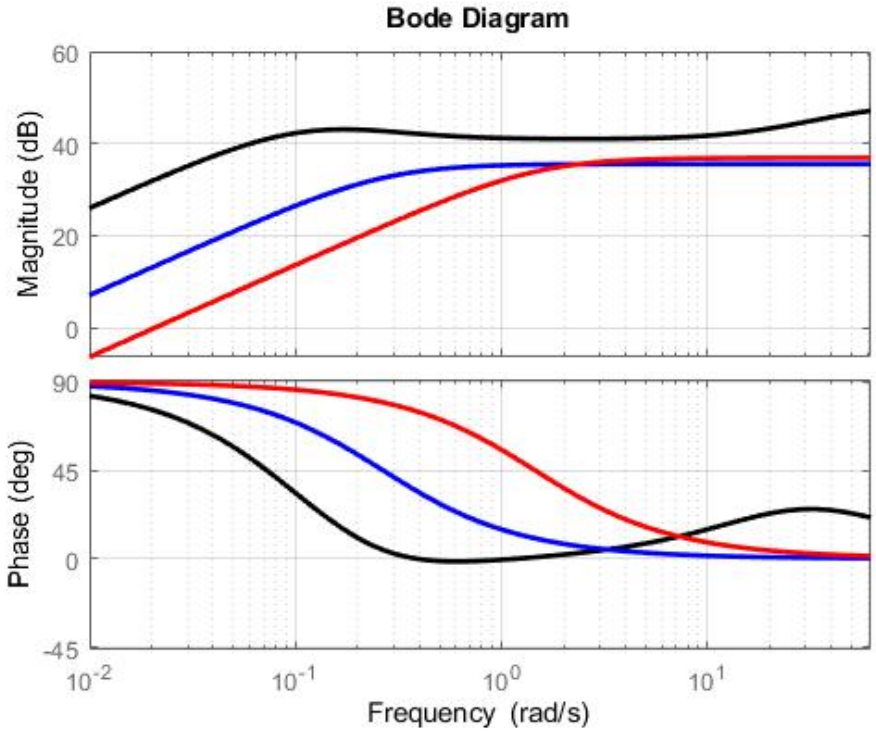

Figure 16: Bode diagrams of the original controller $K(s)$ (black) and of the controllers $K_{new,1}(s)$ (red) and $K_{new,2}(s)$ (blue)

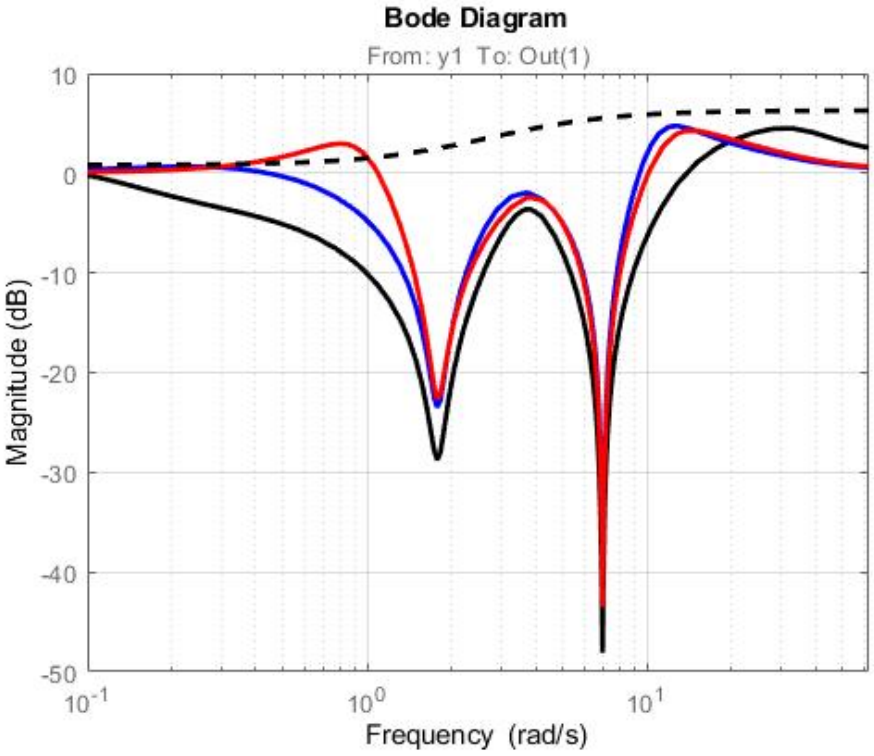

Figure 17: Magnitude plot of $\frac{1}{1+K(z)G(z,\hat{\theta}_N)}$ (black solid), of $\frac{1}{1+K_{new,1}(z)G(z,\hat{\theta}_N)}$ (red solid) and of $\frac{1}{1+K_{new,2}(z)G(z,\hat{\theta}_N)}$ (blue solid) and magnitude plot of the inverse W^{-1} of the weighting W used in (30) (black dashed).

model $G(z,\hat{\theta}_N)$ is here a stable transfer function (unlike the one in Section 5) and that, as shown in Figure 15, $G(z,\hat{\theta}_N)$ presents two sharp resonance peaks. As mentioned above, this model $G(z,\hat{\theta}_N)$ will be used to design a controller entailing less control efforts without (significantly) reducing the damping ability.

The transfer function $\frac{K(z)}{1+K(z)G(z,\hat{\theta}_N)}$ has an H_∞ norm of 326 ($K(z)$ is the discrete-time version of (27)). In order to reduce the control efforts, let us therefore choose $\frac{1}{\gamma} < 326$, say $\gamma = 0.005$.

Using this value of γ, we solve the optimization problem (18)-(19) with the restriction to controllers of the form (21). This leads to a controller $K_{new,1}(s)$:

$$K_{new,1}(s) = k_{w,new,1}\frac{t_{w,new,1}\ s}{t_{w,new,1}\ s+1} \text{ with } k_{w,new,1} = 70.0624 \text{ and } t_{w,new,1} = 0.6876. \tag{28}$$

In Figure 16, we observe that $K_{new,1}(s)$ has a smaller gain than the original controller $K(s)$. The control efforts with this new controller are therefore expected to be smaller. This can also be inferred from the fact that the H_∞ norm of $\frac{K_{new,1}(z)}{1+K_{new,1}(z)G(z,\hat{\theta}_N)}$ is now equal to 114 (recall that it was 272 with (27)).

As far as the damping is concerned, this controller $K_{new,1}(s)$ achieves an even higher damping than the original controller since $\xi_{min}(K_{new,1}, G(z,\hat{\theta}_N)) = 35.7\%$. However, as shown in red in Figure 17, the sensitivity function with $K_{new,1}(z)$ has a peak of amplitude 3 dB at around 0.8 rad/s (0.127 Hz), peak which was not present in the sensitivity function with the original controller (27). Since the sensitivity function is crucial in the disturbance rejection ability of the closed loop (see e.g., (8)), we decide to remove this additional peak. For this purpose, we slightly modify the optimization problem (18)-(19):

$$\arg\ \max_{\tilde{K}}\ \xi_{min}(\tilde{K}(z), G(z,\hat{\theta}_N)) \tag{29}$$

$$\text{subject to } \left\| \begin{pmatrix} \frac{W(z)}{1+\tilde{K}(z)\ G(z,\hat{\theta})} \\ \frac{\gamma\ \tilde{K}(z)}{1+\tilde{K}(z)\ G(z,\hat{\theta})} \end{pmatrix} \right\|_\infty < 1 \tag{30}$$

where the weighting W is chosen as shown in back dashed lines in Figure 17 and where γ remains equal to 0.005. We then solve the optimization problem (29)-(30) and this yields the controller $K_{new,2}(s)$ (whose frequency response is also given in Figure 16):

$$K_{new,2}(s) = k_{w,new,2}\frac{t_{w,new,2}\ s}{t_{w,new,2}\ s+1} \text{ with } k_{w,new,2} = 60.0339 \text{ and } t_{w,new,1} = 3.7582. \tag{31}$$

This controller $K_{new,2}$ presents the desired properties. As shown in blue in Figure 17, the sensitivity function with $K_{new,2}$ does no longer present the resonance peak at 0.8 rad/s. Moreover, $K_{new,2}$ still achieves a very significant damping of $\xi_{min}(K_{new}, G(z,\hat{\theta}_N)) = 29\%$ and the gain of $K_{new,2}$ is similar to the one of $K_{new,1}$ (see Figure 16). The control efforts with $K_{new,2}$ are therefore also expected to be much smaller than with (27): the H_∞ norm of $\frac{K_{new,2}(z)}{1+K_{new,2}(z)G(z,\hat{\theta}_N)}$ is equal to 103 (recall that it was 272 with (27)).

Note that, since these results are already satisfactory, we have decided to not consider the more complex structure (22).

In the next subsection, we will show that the controller (31) indeed entail less control efforts than the original controller (27).

6.4. Verification of the performance of $K_{new,2}(s)$ for large load disturbance on the power system simulation model

In order to perform the validation of the approach proposed in the previous subsection, we apply, at $t = 60\ s$, a large load disturbance p_{load} to the simulation model and, for the sake of completion, we compare the damping ability and the control efforts for three PSS controllers i.e., the original controller (27) and the controllers $K_{new,1}$ and $K_{new,2}$ given in (28) and (31), respectively. This large load disturbance p_{load} has here an amplitude 3.0 $p.u.$ and a duration of 8 cycles.

In Figure 18, we observe that, in the presence of this large disturbance, the new controller $K_{new,2}$ ensures an efficient disturbance rejection: the speed variation is reduced by a factor 10 in two seconds. Due to its highest gain which allows to obtain an even smaller sensitivity function (see Figures 16 and 17), the original controller (27) of course ensures an even better disturbance rejection, but the required control efforts are much higher than with

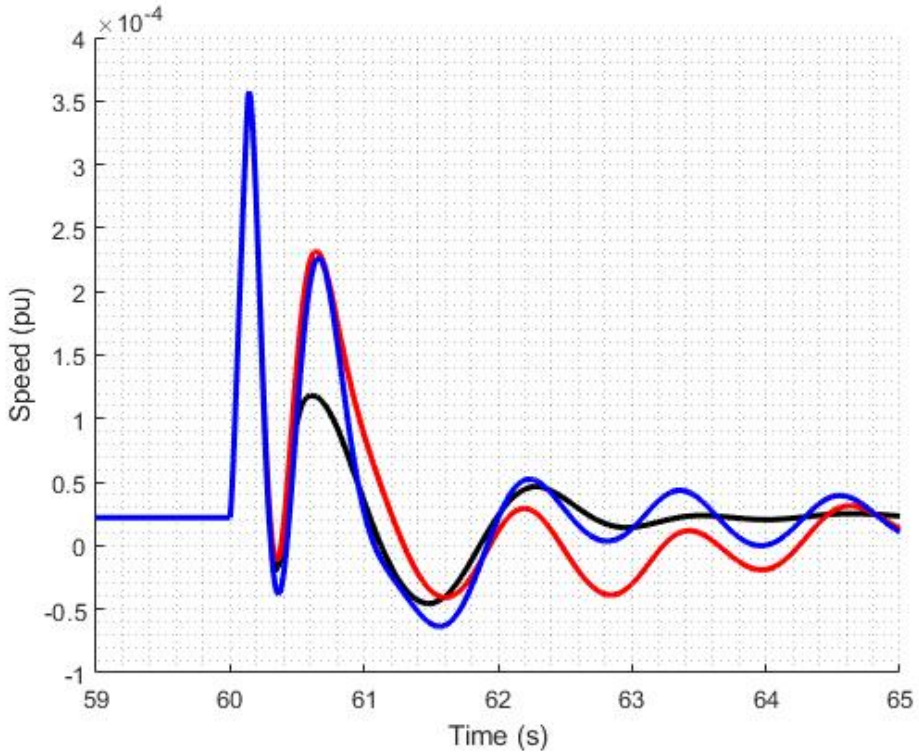

Figure 18: Speed variation of machine 1 with respect to its setpoint when $K(s)$ is used as PSS (black), when $K_{new,1}(s)$ is used as PSS (red) and when $K_{new,2}(s)$ is used as PSS (blue) in the case where a large load disturbance p_{load} of amplitude 3.0 $p.u.$ and with a duration of 8 cycles is applied to the system

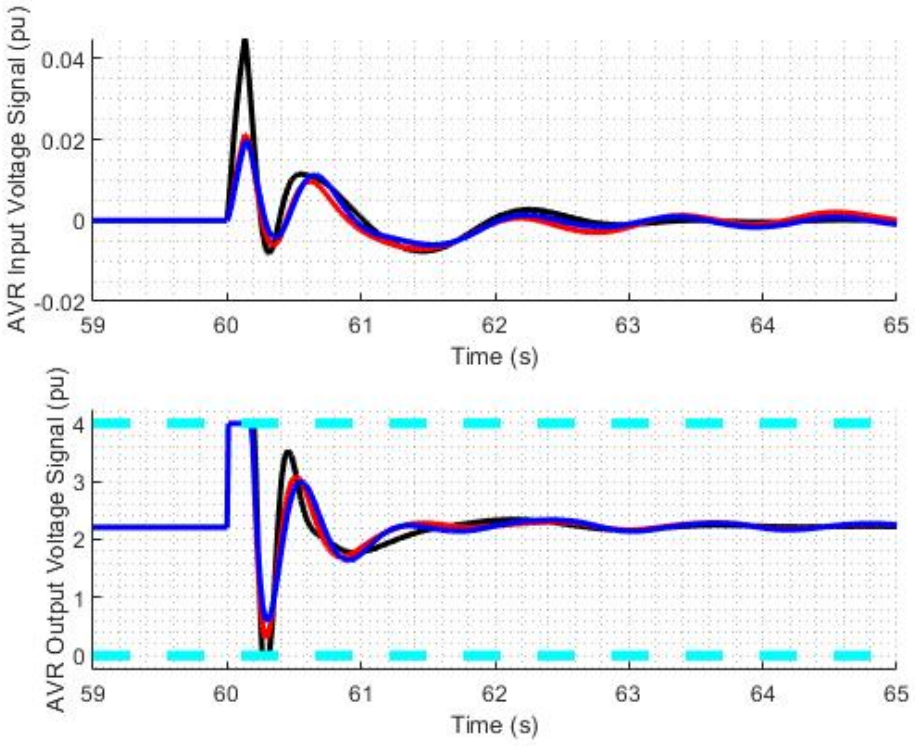

Figure 19: PSS output (top plot) and E_{fd} (bottom plot) of machine 1 when $K(s)$ is used as PSS (black), when $K_{new,1}(s)$ is used as PSS (red) and when $K_{new,2}(s)$ is used as PSS (blue) in the case where a large load disturbance p_{load} of amplitude 3.0 $p.u.$ and with a duration of 8 cycles is applied to the system. The dashed light blue lines in the bottom plot are the AVR limiters (the PSS output limits (i.e. ± 0.2) are here not represented since they are much larger than the actual PSS output).

$K_{new,2}$ (see Figure 19).

When comparing $K_{new,1}$ and $K_{new,2}$, we observe a similar control effort (see Figure 19), but a slightly better disturbance rejection with $K_{new,2}$. The removal of the resonance peak in the sensitivity function has thus been beneficial.

7. Conclusions

Even though the application of Power System Stabilizers for damping power system oscillations is a well established practice in the power industry, keeping these damping controller parameters adequately tuned is still a major challenge as shown in recent major oscillatory incidents in Europe [20, 21]. Unfortunately, these types of events indicate that damping performance, while regularly monitored for entire networks, is not assessed continuously at specific plants, until it is too late, i.e. major incidents occur. While there are well established methods for PSS design based on physics-based power grid simulation models, issues with access, maintenance and update of such models makes the entire PSS tuning process complex and infrequent.

In this paper, an alternative approach based entirely on measurements and system identification techniques is proposed, with the aim of complimenting the existing real-time performance monitoring and PSS redesign methods. In the proposed integrated procedure, damping performance monitoring is applied regularly or is triggered after a major disturbance (e.g. such as a line loss) and injects a low-amplitude probing signal into the machine's AVR that can help to get damping estimates directly related to a specific generator. These estimates are accompanied with a confidence interval, which can help in operator decision making.

One of such decisions would be to improve the controller performance if the monitored damping is too low. To this end, we include in the integrated procedure a method that can help to redesign the PSS parameters such that a better damping performance is achieved. Together with the new parameters, a prediction of the potential damping along with confidence intervals is provided. In other words, before applying the new design, the operator would have a *good idea* of what damping to expect, within a (potentially

small) range. These confidence interval can help the operator decide to apply the new design (or not), e.g. if the uncertainty is low, the new design is safe to apply.

To illustrate the proposed methods, nonlinear simulations were conducted using two different nonlinear power system simulation models driven with stochastic load changes and a probing signal. Using these models we illustrate how the PSS damping performance can be monitored using the application of the probing signal. Note that the amplitude of this probing signal can be made as small as desired by increasing the duration of the probing experiment. Such an approach can be used to minimize the excitation of the system dynamics and to avoid reaching the excitation system limits while at the same time providing the necessary accuracy for the damping estimate. As for the PSS redesign, we illustrate how new PSS designs can be obtained based on the model identified during the probing experiment. Finally, we illustrate how these new control designs perform under large disturbances after being implemented, effectively providing adequate damping when they are needed the most.

Future work will expand this study to address other types of oscillatory phenomena, such as intra-plant oscillations [48] and inter-area oscillations [53] over multiple operating conditions. The approach also needs to be extended to consider coordinated probing for enhanced damping performance monitoring and PSS redesign of both generators [40] and power electronic-based damping control systems [18].

Acknowledgements

The work of L. Vanfretti was supported in part by Dominion Energy Virginia and by Ecole Centrale de Lyon.

Declaration of Competing Interest

The authors declare that they have no known competing financial interests or personal relationships that could have appeared to influence the work reported in this paper.

CRediT authorship contribution statement

Xavier Bombois: Conceptualization; Formal analysis; Investigation; Methodology; Validation; Writing - original draft; Writing, review and editing. **Luigi Vanfretti:** Conceptualization; Formal analysis; Investigation; Methodology; Validation; Writing - original draft; Writing, review and editing.

References

[1] Y. Chompoobutrgool, L. Vanfretti, and M. Ghandhari, "Survey on power system stabilizers control and their prospective applications for power system damping using synchrophasor-based wide-area systems," *European Transactions on Electrical Power*, vol. 21, no. 8, pp. 2098–2111.

[2] L. Angquist and C. Gama, "Damping algorithm based on phasor estimation," in *2001 IEEE Power Engineering Society Winter Meeting. Conference Proceedings (Cat. No.01CH37194)*, vol. 3, 2001, pp. 1160–1165 vol.3.

[3] C. Gama, L. Angquist, G. Ingeström, and M. Noroozian, "Commissioning and operative experience of TCSC for damping power oscillation in the brazilian north-south interconnection," in *CIGRE Session 2020*, 2020.

[4] P. L. Francos, S. S. Verdugo, H. F. Álvarez, S. Guyomarch, and J. Loncle, "INELFE — europe's first integrated onshore HVDC interconnection," in *2012 IEEE Power and Energy Society General Meeting*, 2012, pp. 1–8, ISSN: 1944-9925.

[5] L. Coronado, C. Longás, R. Rivas, S. Sanz, J. Bola, P. Junco, and G. Pérez, "INELFE: main description and operational experience over three years in service," in *2019 AEIT HVDC International Conference (AEIT HVDC)*, 2019, pp. 1–6.

[6] M. Hirose, S. Hara, and Y. Makino, "Outline of the Kii channel HVDC link," in *2001 Power Engineering Society Summer Meeting. Conference Proceedings (Cat. No.01CH37262)*, vol. 1, 2001, pp. 349–362.

[7] K. Uhlen, L. Vanfretti, M. M. de Oliveira, A. B. Leirbukt, V. H. Aarstrand, and J. O. Gjerde, "Wide-Area Power Oscillation Damper implementation and testing in the Norwegian transmission network," in *2012 IEEE Power and Energy Society General Meeting*, 2012, pp. 1–7, ISSN: 1944-9925.

[8] L. Peng, W. Xiaochen, L. Chao, S. Jinghai, H. Jiong, H. Jingbo, Z. Yong, and X. Aidong, "Implementation of CSG's Wide-Area Damping Control System: Overview and experience," in *2009 IEEE/PES Power Systems Conference and Exposition*, 2009, pp. 1–9.

[9] E. Rebello, L. Vanfretti, and M. S. Almas, "Experimental Testing of a Real-Time Implementation of a PMU-Based Wide-Area Damping Control System," *IEEE Access*, vol. 8, pp. 25 800–25 810, 2020.

[10] L. Díez-Maroto, L. Vanfretti, M. S. Almas, G. M. Jónsdóttir, and L. Rouco, "A WACS exploiting generator excitation boosters for power system transient stability enhancement," *Electric Power Systems Research*, vol. 148, pp. 245–253, 2017.

[11] M. S. Almas, M. Baudette, and L. Vanfretti, "Utilizing synchrophasor-based supplementary damping control signals in conventional generator excitation systems," *Electric Power Systems Research*, vol. 157, pp. 157–167, 2018.

[12] L. Vanfretti, G. M. Jónsdóttir, M. S. Almas, E. Rebello, S. R. Firouzi, and M. Baudette, "Audur—a platform for synchrophasor-based power system wide-area control system implementation," *SoftwareX*, vol. 7, pp. 294–301, 2018.

[13] T. H. S. Bossa, N. Martins, R. J. G. C. da Silva, and P. C. Pellanda, "A field test to determine PSS effectiveness at multigenerator power plants," *IEEE Transactions on Power Systems*, vol. 26, no. 3, pp. 1522–1533, 2011.

[14] P. Kundur, G. Berube, L. Hajagos, and R. Beaulieu, "Practical utility experience with and effective use of power system stabilizers," in *2003 IEEE Power Engineering Society General Meeting (IEEE Cat. No.03CH37491)*, vol. 3, 2003, pp. 1777–1785.

[15] D. C. Lee, R. E. Beaulieu, and J. Service, "A Power System Stabilizer Using Speed and Electrical Power Inputs — Design and Field Experience," *IEEE Power Engineering Review*, vol. PER-1, no. 9, pp. 28–29, 1981.

[16] Excitation Systems Subcommittee, "IEEE Tutorial Course Power System Stabilization via Excitation Control," *IEEE Power and Energy Society*, no. 09TP250, p. 74, 2009.

[17] R. Jankowski, B. Sobczak, and R. Trebski, "Impact of the Polish tielines outages on the inter-area oscillations pattern in the synchronous system of continental Europe," *Acta Energetica*, no. 2, pp. 89–97, 2017.

[18] J. C. R. Ferraz, N. Martins, and G. N. Taranto, "Coordinated stabilizer tuning in large power systems considering multiple operating conditions," in *2007 IEEE Power Engineering Society General Meeting*, 2007, pp. 1–8, ISSN: 1932-5517.

[19] H. Saad, S. Dennetière, and B. Clerc, "Interactions investigations between power electronics devices embedded in HVAC network," in *13th IET International Conference on AC and DC Power Transmission (ACDC 2017)*, 2017, pp. 1–7.

[20] ENTSO-E Sub-Group System Dynamics and Protection, "Analysis of CE Inter-Area Oscillations of 1st December 2016," *ENTSO-E*, 2017, Available online: https://tinyurl.com/ENTSOE2016, Accessed: June 28, 2022.

[21] ——, "Oscillation Event 03.12.2017," 2018, Available online: https://tinyurl.com/ENTSOE2017, Accessed: June 28, 2022.

[22] ICS Investigation Expert Panel, "Continental Europe Synchronous Area Separation on 08 January 2021," *ENTSO-E*, p. 144, 2021, Available online: https://tinyurl.com/ENTSOE2021, Accessed: June 28, 2022.

[23] O. Butkevych and V. Chyzhevskyi, "Some features of electromechanical oscillations modes identification in power systems," in *Power Systems Research and Operation: Selected Problems*, ser. Studies in Systems, Decision and Control, O. Kyrylenko, A. Zharkin, O. Butkevych, I. Blinov, I. Zaitsev, and A. Zaporozhets, Eds. Springer International Publishing, 2022, pp. 47–70.

[24] D. Kosterev, C. Taylor, and W. Mittelstadt, "Model validation for the august 10, 1996 WSCC system outage," *IEEE Transactions on Power Systems*, vol. 14, no. 3, pp. 967–979, 1999.

[25] J. Undrill, L. Pereira, D. Kosterev, S. Patterson, D. Davies, S. Yang, and B. Agrawal, "Generating unit model validation: WECC lessons and moving forward," in *2009 IEEE Power & Energy Society General Meeting*, 2009, pp. 1–5, ISSN: 1932-5517.

[26] T. Bogodorova, L. Vanfretti, V. S. Perić, and K. Turitsyn, "Identifying uncertainty distributions and confidence regions of power plant parameters," *IEEE Access*, vol. 5, pp. 19 213–19 224, 2017.

[27] A. Semerow, S. Höhn, M. Luther, W. Sattinger, H. Abildgaard, A. D. Garcia, and G. Giannuzzi, "Dynamic study model for the interconnected power system of continental europe in different simulation tools," in *2015 IEEE Eindhoven PowerTech*, pp. 1–6.

[28] L. Vanfretti, L. Dosiek, J. W. Pierre, D. Trudnowski, J. H. Chow, R. García-Valle, and U. Aliyu, "Application of ambient analysis techniques for the estimation of electromechanical oscillations from measured PMU data in four different power systems," *European Transactions on Electrical Power*, vol. 21, no. 4, pp. 1640–1656, 2011.

[29] V. S. Perić and L. Vanfretti, "Power System Ambient Mode Estimation Considering Spectral Load Properties," *IEEE Transactions on Power Systems*, vol. 29, no. 3, pp. 1133–1143.

[30] L. Rydin Gorjão, L. Vanfretti, D. Witthaut, C. Beck, and B. Schäfer, "Phase and Amplitude Synchronization in Power-Grid Frequency Fluctuations in the Nordic Grid," *IEEE Access*, vol. 10, pp. 18 065–18 073, 2022.

[31] C. Wang, L. Vanfretti, C. Mishra, K. D. Jones, and R. M. Gardner, "Identifying oscillations injected by inverter-based solar energy sources," 2022. [Online]. Available: https://arxiv.org/abs/2202.11579

[32] M. de Castro, L. Vanfretti, C. Mishra, X. Xu, and K. D. Jones, "Experiences with Dynamical Mode Decomposition for Wide-Area Mode Estimation," in *Proceedings of the 10th Workshop on Modelling and*

Simulation of Cyber-Physical Energy Systems (MSCPES), 2022, pp. 1–6.

[33] L. Ljung, *System Identification: Theory for the User, 2nd Edition*. Englewood Cliffs, NJ: Prentice-Hall, 1999.

[34] N. Zhou, J. Pierre, and J. Hauer, "Initial results in power system identification from injected probing signals using a subspace method," *IEEE Transactions on Power Systems*, vol. 21, no. 3, pp. 1296–1302, 2006.

[35] V. Perić, X. Bombois, and L. Vanfretti, "Optimal multisine probing signal design for power system electromechanical mode estimation," in *Proceedings of the 50th Hawaii International Conference on System Sciences*, 2017.

[36] S. Boersma, X. Bombois, L. Vanfretti, J.-C. Gonzalez-Torres, and A. Benchaib, "Probing signal design for enhanced damping estimation in power networks," *International Journal of Electrical Power & Energy Systems*, vol. 129, p. 106640, 2021.

[37] G. Zhang, W. Hu, D. Cao, Q. Huang, J. Yi, Z. Chen, and F. Blaabjerg, "Deep reinforcement learning-based approach for proportional resonance power system stabilizer to prevent ultra-low-frequency oscillations," *IEEE Transactions on Smart Grid*, vol. 11, no. 6, pp. 5260–5272, 2020.

[38] G. Zhang, W. Hu, D. Cao, Q. Huang, Z. Chen, and F. Blaabjerg, "A novel deep reinforcement learning enabled sparsity promoting adaptive control method to improve the stability of power systems with wind energy penetration," *Renewable Energy*, vol. 178, pp. 363–376, 2021. [Online]. Available: https://www.sciencedirect.com/science/article/pii/S0960148121009484

[39] J. Chow, G. Boukarim, and A. Murdoch, "Power system stabilizers as undergraduate control design projects," *IEEE Transactions on Power Systems*, vol. 19, no. 1, pp. 144–151, 2004.

[40] G. Boukarim, S. Wang, J. Chow, G. Taranto, and N. Martins, "A comparison of classical, robust, and decentralized control designs for multiple power system stabilizers," *IEEE Transactions on Power Systems*, vol. 15, no. 4, pp. 1287–1292, 2000.

[41] A. C. Zolotas, P. Korba, B. Chaudhuri, and I. M. Jaimoukha, "H2 lmi-based robust control for damping oscillations in power systems," in *2007 IEEE International Conference on System of Systems Engineering*. IEEE, 2007, pp. 1–8.

[42] S. Boersma, L. Vanfretti, and A. Benchaib, "Enhanced LMI-based damping control in power networks through a high voltage direct current line," in *2021 European Control Conference (ECC)*, pp. 2098–2103.

[43] V. S. Perić, X. Bombois, and L. Vanfretti, "Optimal signal selection for power system ambient mode estimation using a prediction error criterion," *IEEE Transactions on Power Systems*, vol. 31, no. 4, pp. 2621–2633, 2016.

[44] K. Zhou and J. Doyle, *Essentials of Robust Control*. Prentice Hall, Upper Saddle River, New Jersey, 1998.

[45] M. Chilali and P. Gahinet, "H_∞ design with pole placement constraints: an lmi approach," *IEEE Transactions on automatic control*, vol. 41, no. 3, pp. 358–367, 1996.

[46] M. A. Gelbart, J. Snoek, and R. P. Adams, "Bayesian optimization with unknown constraints," *arXiv preprint arXiv:1403.5607*, 2014.

[47] M. Baur, M. Otter, and B. Thiele, "Modelica Libraries for Linear Control Systems," in *7th International Modelica Conference*, ser. 43. Linköping Electronic Conference Proceedings, 2009, pp. 593–602.

[48] F. D. Marco, P. Rullo, and N. Martins, "Synthetic power system models for PSS tuning and performance assessment," in *2021 IEEE Electrical Power and Energy Conference (EPEC)*, pp. 107–112, ISSN: 2381-2842.

[49] M. de Castro, D. Winkler, G. Laera, L. Vanfretti, S. Dorado-Rojas, T. Rabuzin, B. Mukherjee, and M. Navarro, "Version OpenIPSL 2.0.0-iTesla power systems library (iPSL): A Modelica library for phasor time-domain simulations"," *SoftwareX*, vol. 21, 2023.

[50] A. Klöckner, A. Knoblach, and A. Heckmann, "How to shape noise spectra for continuous system simulation," *Mathematical and Computer Modelling of Dynamical Systems*, vol. 23, no. 3, pp. 284–300, 2017.

[51] X. Bombois, B. Anderson, and M. Gevers, "Quantification of frequency domain error bounds with guaranteed confidence level in prediction error identification," *Systems and Control Letters*, vol. 54, no. 5, pp. 471–482, 2005.

[52] P. Kundur, *Power system stability and control*. McGraw-Hill, 1994.

[53] Y. Chompoobutrgool and L. Vanfretti, "Using PMU signals from dominant paths in power system wide-area damping control," *Sustainable Energy, Grids and Networks*, vol. 4, pp. 16–28.